Article

Developmental Cell

Hemodynamic Forces Sculpt Developing Heart Valves through a KLF2-WNT9B Paracrine Signaling Axis

Graphical Abstract

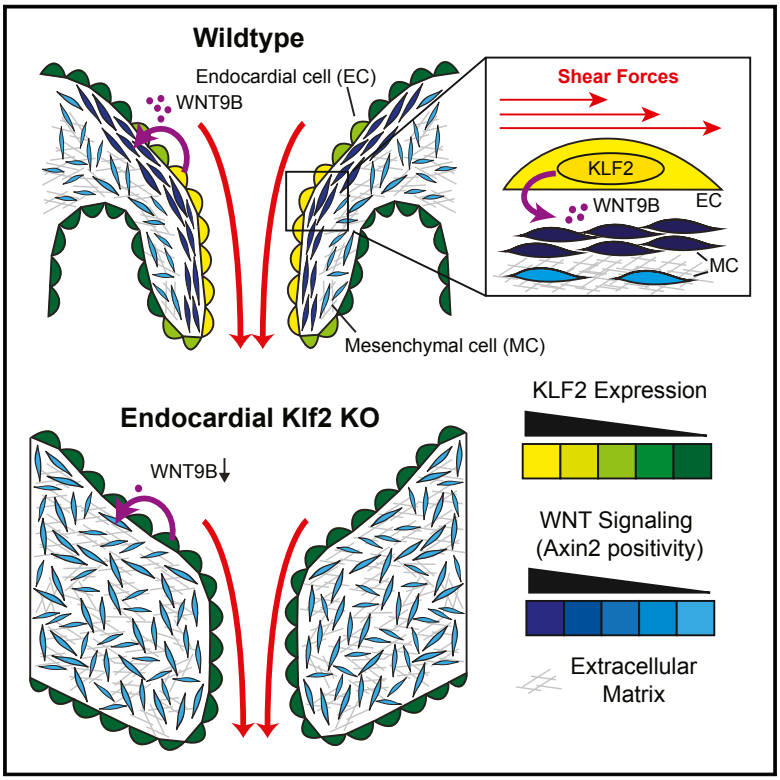

Highlights

- Endocardial KLF2 is expressed in a dynamic pattern predicted by hemodynamic forces
- Endocardial deletion of *Klf2* results in altered cardiac cushion remodeling
- KLF2 regulates endocardial *Wnt9b* expression, which alters cushion mesenchyme
- *wnt9b* is regulated by hemodynamic forces in the developing zebrafish heart

Authors

Lauren M. Goddard, Anne-Laure Duchemin, Harini Ramalingan, ..., Bin Zhou, Julien Vermot, Mark L. Kahn

Correspondence

markkahn@pennmedicine.upenn.edu

In Brief

How cardiac cushions are remodeled into mature valve leaflets is not well understood. Goddard et al. find that hemodynamic forces drive expression of KLF2 by the cardiac endocardium. Through a cell non-autonomous mechanism, *Klf2* regulates the WNT ligand, *Wnt9b*, which acts on neighboring mesenchymal cells to control cushion remodeling.

Goddard et al., 2017, Developmental Cell *43*, 1–16
November 6, 2017
https://doi.org/10.1016/j.devcel.2017.09.023

CellPress

Please cite this article in press as: Goddard et al., Hemodynamic Forces Sculpt Developing Heart Valves through a KLF2-WNT9B Paracrine Signaling Axis, Developmental Cell (2017), https://doi.org/10.1016/j.devcel.2017.09.023

Developmental Cell
Article

Hemodynamic Forces Sculpt Developing Heart Valves through a KLF2-WNT9B Paracrine Signaling Axis

Lauren M. Goddard,[1] Anne-Laure Duchemin,[2,7,8,9] Harini Ramalingan,[3] Bingruo Wu,[4] Mei Chen,[1] Sharika Bamezai,[1] Jisheng Yang,[1] Li Li,[1] Michael P. Morley,[1] Tao Wang,[1] Marielle Scherrer-Crosbie,[1] David B. Frank,[5] Kurt A. Engleka,[1] Stephen C. Jameson,[6] Edward E. Morrisey,[1] Thomas J. Carroll,[3] Bin Zhou,[4] Julien Vermot,[2,7,8,9] and Mark L. Kahn[1,10,*]
[1]Department of Medicine and Cardiovascular Institute, University of Pennsylvania, 3400 Civic Center Boulevard, Philadelphia, PA 19104, USA
[2]Institut de Génétique et de Biologie Moléculaire et Cellulaire, Illkirch 67404, France
[3]Department of Internal Medicine (Nephrology) and Molecular Biology, University of Texas Southwestern Medical Center, 5323 Harry Hines Boulevard, Dallas, TX 75390, USA
[4]Department of Genetics, Pediatric, and Medicine (Cardiology) and Wilf Cardiovascular Research Institute, Albert Einstein College of Medicine of Yeshiva University, 1301 Morris Park Avenue, Bronx, NY 10461, USA
[5]Division of Pediatric Cardiology, Department of Pediatrics, The Children's Hospital of Philadelphia, Philadelphia, PA 19104, USA
[6]Department of Laboratory Medicine and Pathology, Center for Immunology, University of Minnesota, Minneapolis, MN, USA
[7]Centre National de la Recherche Scientifique, UMR7104, Illkirch 67404, France
[8]Institut National de la Santé et de la Recherche Médicale, U964, Illkirch 67404, France
[9]Université de Strasbourg, Illkirch 67404, France
[10]Lead Contact
*Correspondence: markkahn@pennmedicine.upenn.edu
https://doi.org/10.1016/j.devcel.2017.09.023

SUMMARY

Hemodynamic forces play an essential epigenetic role in heart valve development, but how they do so is not known. Here, we show that the shear-responsive transcription factor KLF2 is required in endocardial cells to regulate the mesenchymal cell responses that remodel cardiac cushions to mature valves. Endocardial *Klf2* deficiency results in defective valve formation associated with loss of *Wnt9b* expression and reduced canonical WNT signaling in neighboring mesenchymal cells, a phenotype reproduced by endocardial-specific loss of *Wnt9b*. Studies in zebrafish embryos reveal that *wnt9b* expression is similarly restricted to the endocardial cells overlying the developing heart valves and is dependent upon both hemodynamic shear forces and *klf2a* expression. These studies identify KLF2-WNT9B signaling as a conserved molecular mechanism by which fluid forces sensed by endothelial cells direct the complex cellular process of heart valve development and suggest that congenital valve defects may arise due to subtle defects in this mechanotransduction pathway.

INTRODUCTION

Heart valves ensure that the beating heart drives unidirectional blood flow. Valve function must be mechanically flawless, as the heart beats continuously and either obstruction of forward flow or backward regurgitation of blood due to a defective valve can result in heart failure. Heart valve defects are among the most common human congenital anomalies, with an incidence of approximately 2% of live births (Hoffman and Kaplan, 2002). Although some valvular heart defects have been linked to specific genetic mutations (e.g., in *NOTCH1*, *TBX5*, *GATA4*, *TBX20*, *LMCD1*, *TNS1*, and *DCHS1*) (Dina et al., 2015; Durst et al., 2015; Garg et al., 2005; Richards and Garg, 2010; Theodoris et al., 2015), the majority have no clearly definable genetic or environmental cause (Levine et al., 2015). Thus, it is thought that epigenetic factors play an important role in the pathogenesis of congenital valve defects.

Heart valve development in the mouse begins at E9.5–10.5 with the formation of cardiac cushions at the sites of future atrioventricular (AV) and outflow tract (OFT) valves (Gitler et al., 2003; MacGrogan et al., 2014). Cushion formation begins with endocardial-mesenchymal transformation (EMT), a process in which endocardial cells delaminate from an organized cell layer, transform into mesenchymal cells, and invade the matrix that separates the endocardial and myocardial cell layers (Markwald et al., 1977). In addition to their contribution to future valves, cardiac cushions also form the membranous septum and basal parts of the aortic and pulmonic outflow tracts. Following completion of EMT, the bulky cardiac cushions are gradually remodeled to mature valves with thin, perfectly co-apting leaflets (MacGrogan et al., 2014). Although the processes of EMT and cushion formation have been elucidated in significant molecular and cellular detail (reviewed in von Gise and Pu, 2012), the mechanisms that underlie subsequent remodeling to mature valves remain poorly understood. Since genetically modified mice with defects in EMT rarely survive to birth, it is likely that most human congenital heart valve defects reflect defects in cushion remodeling rather than cushion formation.

Early studies of heart development in the chick embryo noted that the future outflow tracts of the heart formed along lines defined by visibly distinct streams of blood (Jaffee, 1965), suggesting that blood flow may be an important epigenetic regulator of heart development. Direct evidence for this hypothesis has come from studies in both chick and zebrafish embryos in

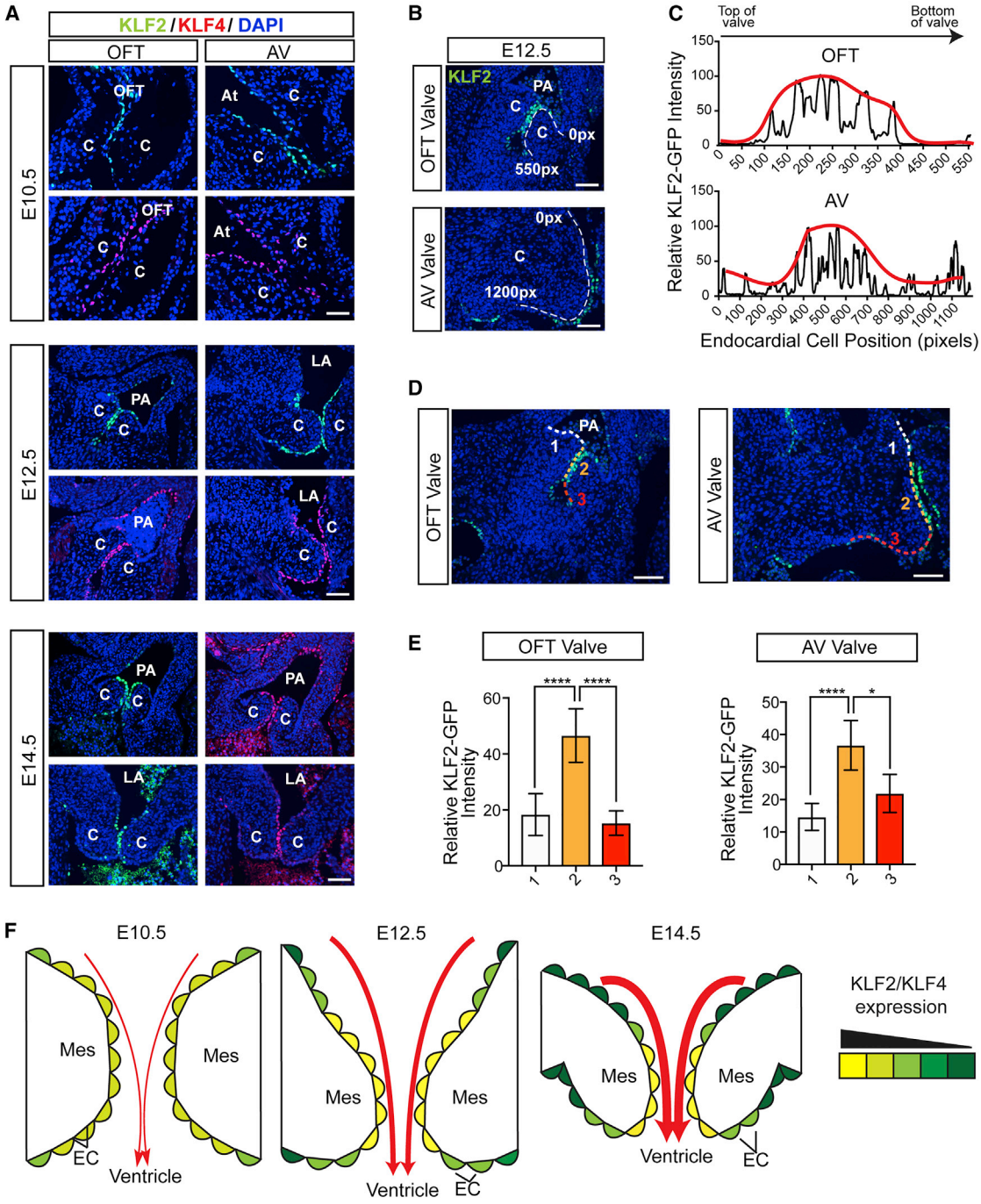

Figure 1. Graded Expression of KLF2 and KLF4 in the Endocardial Cells of the Remodeling Cardiac Cushions

(A) KLF2 (green) and KLF4 (red) expression in developing heart valves were detected by immunostaining GFP-KLF2 hearts at E10.5, E12.5, and E14.5 with anti-GFP and anti-KLF4 antibodies. DAPI (blue) denotes nuclei. Scale bar represents 70μm at E10.5 and 100 μm at E12.5 and E14.5.

(B) Representative images showing how endocardial cell GFP-KLF2 (green) intensity along the cushion endocardium was calculated. White dotted lines indicate the relative positions of endocardial cells measured in pixels. Scale bar represents 100 μm.

(C) Representative plots showing endocardial GFP-KLF2 intensity across the OFT and AV cushions shown in (B).

(D and E) Quantitation of variable, spatially determined GFP-KLF2 expression in the developing E12.5 valves. Representative images of OFT and AV valves depicting how the KLF2-GFP (green) was quantified based on three defined zones as shown in (D): 1, artery/atrial side (predicted to have lower shear forces); 2, area of valve leaflet contact (predicted to have higher shear forces); 3, ventricular side (predicted to have lower shear forces). Scale bar represents 100 μm.

(legend continued on next page)

which mechanical alteration of blood flow conferred cardiac defects, many involving valve development and function (Hogers et al., 1999; Hove et al., 2003; Sedmera et al., 1999; Vermot et al., 2009; Yalcin et al., 2010). Mechanical blockade of blood flow through the developing fish heart or alteration in fluid shear forces achieved by changing blood viscosity or cardiac contractile function disrupt valve formation (Hove et al., 2003; Vermot et al., 2009). Similarly, conotruncal banding or ligation of major blood vessels leads to valve malformations and septal defects in chick embryos (Hogers et al., 1999; Sedmera et al., 1999). Extending these studies to mammals has been difficult, however, because lack of blood flow results in embryonic lethality by E10 in the mouse (Wakimoto et al., 2000), a time point prior to cushion remodeling and mature valve formation.

The molecular pathway(s) by which blood flow and hemodynamic forces regulate heart valve development remain poorly understood. Expression of the transcription factor KLF2 is regulated by fluid shear in cultured human endothelial cells *ex vivo* and in mouse and human vascular endothelium *in vivo* (Dekker et al., 2002, 2005; Lee et al., 2006; Parmar et al., 2005; Zhou et al., 2015). In the developing zebrafish heart, *klf2a* is strongly expressed in endothelial cells overlying the developing valve and strictly dependent upon hemodynamic forces, and loss of *klf2a* confers valve defects like those observed with loss of blood flow or shear (Heckel et al., 2015; Steed et al., 2016; Vermot et al., 2009). Whether KLF2 plays a similar requisite role in mammalian heart development and, more importantly, whether and how information from hemodynamic forces sensed by endocardial cells in contact with blood might be relayed through KLF2 to instruct underlying cells not exposed to blood during the development of heart valves is unknown.

In the present study, we demonstrate that KLF2 and KLF4, related shear-responsive transcription factors (Clark et al., 2011; McCormick et al., 2001; Zhou et al., 2015), are required in the endocardium of the developing mouse heart during the remodeling of cardiac cushions to mature heart valves. The action of these endocardial transcription factors is mediated primarily by WNT9B, a secreted protein that acts on underlying mesenchymal cells through canonical WNT signals. Analysis of zebrafish embryos reveals that this pathway is conserved during fish heart valve development, and that endocardial *wnt9b* expression is dependent upon hemodynamic forces and *klf2a*. Our studies identify a KLF-WNT signaling axis through which hemodynamic forces are converted by endocardial cells to paracrine WNT signals that orchestrate the behavior of cells not in contact with blood to form a mature heart valve. This pathway provides an elegant epigenetic mechanism by which valve development may be precisely tailored by blood flow to create perfectly functioning heart valves, and suggests that small errors in the transmission of such signals may result in congenital valve disease.

RESULTS

Endocardial KLF2 and KLF4 Are Expressed in a Dynamic Pattern Predicted by Hemodynamic Shear Forces during Cushion Remodeling

KLF2 expression in endothelial cells is tightly regulated by fluid shear forces *in vitro* (Clark et al., 2011; Dekker et al., 2002; Huddleson et al., 2004; Parmar et al., 2006; Zhou et al., 2015) and *in vivo*, where spatial resolution is exquisite, and significant changes in KLF2 expression have been observed between adjacent endothelial cells in association with shifting hemodynamic forces at sites of vascular bifurcation (Clark et al., 2011; Dekker et al., 2002; Groenendijk et al., 2005; Huddleson et al., 2004; Parmar et al., 2006; Zhou et al., 2015). The related transcription factor KLF4 is less studied in the endothelium, but is also upregulated by fluid shear forces in endothelial cells *in vitro* and regulated by the same shear-responsive MEKK3-ERK5 pathway as KLF2 in endocardial cells *in vivo* (Clark et al., 2011; Zhou et al., 2015). Prior studies by us and others have demonstrated that *Klf2* mRNA expression in the developing heart is endocardial specific and becomes progressively restricted to the endocardial cells overlying the developing cushions and valves during mid-late gestation (Heckel et al., 2015; Lee et al., 2006). To further characterize KLF2 expression in the developing heart, we used anti-GFP antibodies to detect a GFP-KLF2 fusion protein expressed from the endogenous *Klf2* locus (Weinreich et al., 2009). GFP-KLF2 was expressed in the endothelial cells lining the cardiac cushions after E10.5, but not in underlying cushion mesenchymal cells (Figure 1A). Quantitative analysis revealed that between E10.5 and E14.5, GFP-KLF2 expression in cushion endocardial cells demonstrated a progressively graded pattern in which the greatest GFP-KLF2 expression was localized to the central part of the developing cushions, the site at which blood flows through the narrowest channel and shear forces are predicted to be highest (Figures 1A–1E). A small amount of GFP-KLF2 expression was also detected in ventricular endocardial cells, particularly those at the trabecular tips that are also predicted to be exposed to shear forces, but ventricular GFP-KLF2 expression was extinguished by E14.5 (Figure S1A).

We and others have demonstrated that expression of the KLF2-related transcription factor KLF4 is also upregulated by fluid shear forces in endothelial cells *in vitro* and activated by the same upstream MAPK pathway as KLF2 in endothelial cells *in vivo* (Clark et al., 2011; Zhou et al., 2015). Anti-KLF4 antibody staining revealed that KLF4 expression mirrored that of KLF2, i.e., was specific to the endothelial cells lining the cardiac cushions and distributed in a graded manner consistent with predicted shear forces (Figure 1A). These studies demonstrate that KLF2 and KLF4 are expressed in a highly graded fashion in endothelial cells lining the cardiac cushions (Figure 1F), and suggest that they may function in transducing endothelial cell

KLF2-GFP quantitation of the areas defined in (D) is shown in (E). Error bars represent ±SEM, *p ≤ 0.05, ****p ≤ 0.0001 using an unpaired two-tailed Student's t test (n = 4–5 from at least 2 litters).

(F) Schematic depiction of KLF2/KLF4 expression in the endocardium overlying the developing AV valve between E10.5 and E14.5. The thickness of the red arrows indicates the relative strength of hemodynamic shear forces.

At, atrium; C, cushion; EC, endocardial cell; LA, left atrium; Mes, mesenchyme; OFT, outflow tract; PA, pulmonary artery. See also Figure S1.

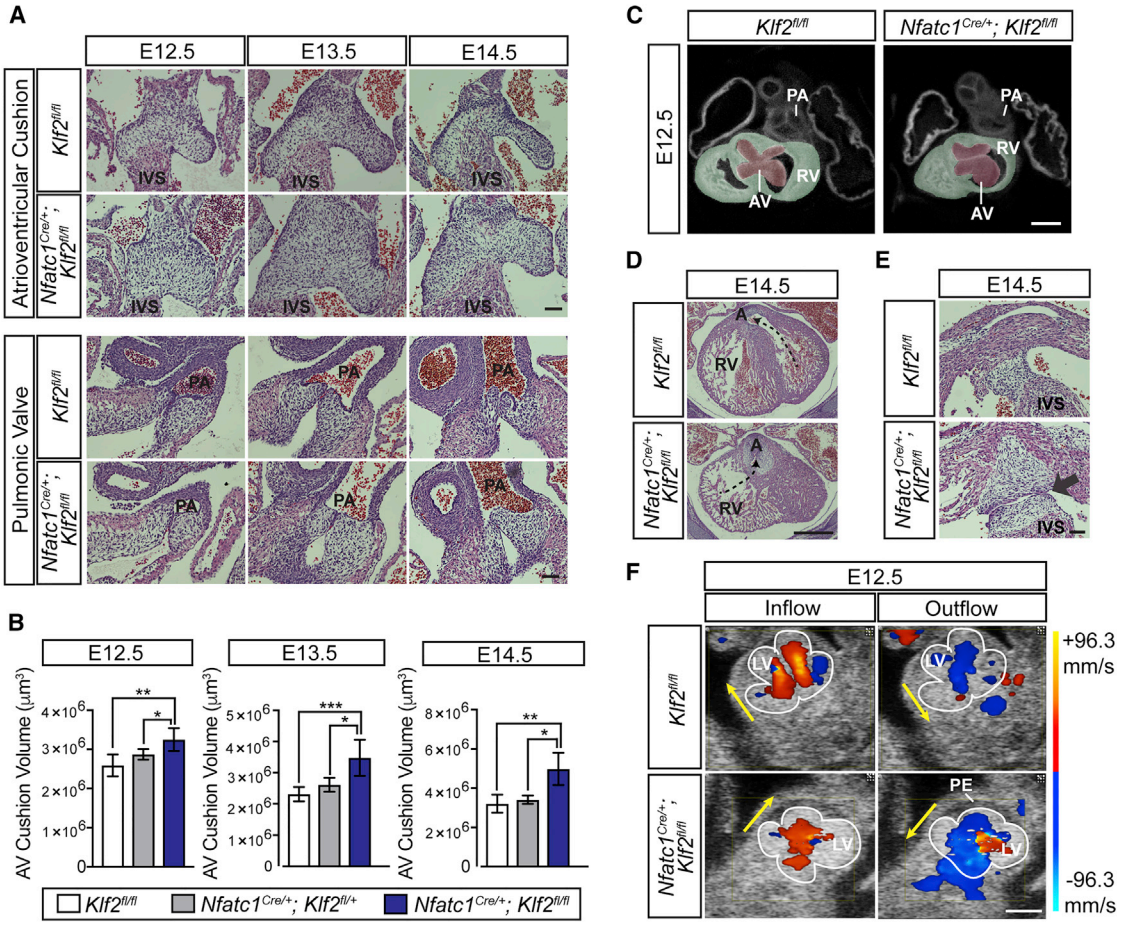

Figure 2. Endocardial Loss of *Klf2* Results in Cardiac Cushion Defects and Abnormal Intracardiac Blood Flow

(A) H&E staining of cardiac cushions in *Nfatc1*$^{Cre/+}$; *Klf2*$^{fl/fl}$ and littermate control hearts between E12.5 and E14.5. Scale bar represents 100 μm.

(B) Quantitation of AV cushion volume in E12.5–E14.5 *Nfatc1*$^{Cre/+}$; *Klf2*$^{fl/fl}$ mice compared with controls. Error bars represent ±SEM, *p ≤ 0.05, **p ≤ 0.01, ***p ≤ 0.001 using an unpaired two-tailed Student's t test (n = 3–7 from 3 to 4 litters).

(C) Optical tomography 2D X-axis images of E12.5 *Nfatc1*$^{Cre/+}$; *Klf2*$^{fl/fl}$ hearts compared with controls. Red and green structures represent the atrioventricular cushion and ventricular myocardium, respectively. Scale bar represents 200 μm.

(D) H&E images demonstrating the presence of DORV in *Nfatc1*$^{Cre/+}$; *Klf2*$^{fl/fl}$ mice. Dotted lines denote the path of blood flow from the ventricle to the aorta in control and *Nfatc1*$^{Cre/+}$; *Klf2*$^{fl/fl}$ animals. Scale bar represents 500 μm.

(E) H&E staining of the membranous septum in E14.5 control and *Nfatc1*$^{Cre/+}$; *Klf2*$^{fl/fl}$ animals. Arrow indicates a septal defect in a *Nfatc1*$^{Cre/+}$; *Klf2*$^{fl/fl}$ heart. Scale bar represents 100 μm.

(F) Color Doppler of E12.5 control and *Nfatc1*$^{Cre/+}$; *Klf2*$^{fl/fl}$ littermates. Yellow arrows indicate the direction of blood flow. Solid white lines outline the fetal heart. Scale bar represents 500 μm.

A, aorta; AV, atrioventricular cushion; IVS, interventricular septum; LV, left ventricle; PA, pulmonary artery; PE, pericardial edema; RV, right ventricle. See also Figures S1 and S2; Movies S1, S2, S3, and S4; Table S1.

responses to fluid shear forces during the remodeling of cushions to mature heart valves.

Klf2 Is Required in the Endocardium for Cushion Remodeling during Heart Valve Development

To functionally test the role of KLF2 specifically in the developing heart, we used an Nfatc1-Cre allele that expresses Cre recombinase in the endocardium of the heart but not in the peripheral vascular endothelium (Wu et al., 2012). Intercrossing *Nfatc1*$^{Cre/+}$; *Klf2*$^{fl/+}$ and *Klf2*$^{fl/fl}$ animals revealed no *Nfatc1*$^{Cre/+}$; *Klf2*$^{fl/fl}$ (Nfatc1 Klf2 KO) animals at birth, and timed matings demonstrated embryonic loss of most Nfatc1 Klf2 KO animals by E14.5 (Table S1). Analysis of Nfatc1 Klf2 KO embryo hearts revealed significant defects in AV and OFT cushion remodeling, while myocardial growth appeared normal until the onset of heart failure, when the ventricular wall exhibited significant thinning (Figures 2 and S1B). Cardiac cushions were histologically indistinguishable from those in control embryos until E12.5, when Nfatc1 Klf2 KO AV and OFT cushions exhibited notably larger volumes than those in control littermates (Figures 2A–2C). Nfatc1 Klf2 KO cushions also failed to thin and elongate in the direction of flow in a manner similar to control cushions (Figure 2A).

Early in cardiac development (prior to E14.5 in the mouse), both the aortic and pulmonic outflow tracts arise from the right

ventricle, while subsequent remodeling of the AV cushion creates a separate aortic outflow tract from the left ventricle (Lin et al., 2012). Consistent with a failure of cushion remodeling, the aortic OFT of E14.5 Nfatc1 Klf2 KO hearts failed to connect to the left ventricle (thus maintaining a double outlet right ventricle [DORV]) (Figure 2D), and all Nfatc1 Klf2 KO animals surviving to E14.5 exhibited a membranous septal defect (Figure 2E; Movies S1 and S2).

The observed defects in cushion remodeling suggested that Nfatc1 Klf2 KO embryos die in mid-gestation due to failure of the developing valves to support the requirement for increasing blood flow in the embryo. We have previously demonstrated that embryos lacking *Klf2* in all endothelial cells (Tie2 Klf2 KOs) exhibit increased systolic stroke volumes and death due to high output heart failure (Lee et al., 2006). These findings were attributed to abnormal blood vessel tone because lethality was rescued by alpha adrenergic agonists that act selectively on peripheral vascular smooth muscle in adult animals. However, high output heart failure may also arise due to defective heart valves, and alpha adrenergic rescue may be explained by the transient expression of alpha adrenergic receptors in embryonic myocardial cells (Lin et al., 1992). Doppler analysis at E12.5 revealed augmented ventricular outflow in Nfatc1 Klf2 KO hearts compared with controls (Figure 2F; Movies S3 and S4), findings consistent with high cardiac output. These observations suggest that the defective cushion remodeling observed in mid-gestation Nfatc1 Klf2 KO embryos is associated with abnormal valve function and hemodynamic changes, resulting in embryonic lethality due to heart failure.

Although KLF4 is expressed in the cushion endocardium in a pattern similar to KLF2 (Figure 1A), mice lacking KLF4 survive to birth with no apparent cardiovascular defects (Segre et al., 1999), and a role for KLF4 in heart development has not been defined. To test whether KLF2 and KLF4 play overlapping roles during heart valve development, we generated mice with endocardial-specific deletion of both alleles of *Klf4* and one allele of *Klf2*. *Nfatc1*$^{Cre/+}$; *Klf2*$^{fl/+}$; *Klf4*$^{fl/fl}$ mice exhibited mid-gestation lethality associated with cushion defects, DORV, and membranous septal defects identical to those observed in Nfatc1 Klf2 KO embryos (Figure S2). These studies demonstrate that the shear-regulated transcription factors KLF2 and KLF4 are expressed in the endothelial cells lining the cardiac cushions in a manner proportional to predicted shear forces, and play essential roles in the remodeling processes required for valve and outflow tract development in the heart.

Klf2 Is Required in Cushion Endocardium and Not Mesenchyme during Remodeling

Since the Nfatc1-Cre allele drives gene deletion prior to EMT (Wu et al., 2012), it is possible that the mesenchymal defects observed in Nfatc1 Klf2 KO embryos reflect a requirement for KLF2 in mesenchymal rather than endocardial cells. To test the requirement for KLF2 in cushion mesenchymal cells, we generated *Dermo1*$^{Cre/+}$; *Klf2*$^{fl/fl}$ (Dermo1 Klf2 KO) animals in which KLF2 was deleted immediately after the onset of EMT and expression of *Dermo1* (aka *Twist2*). Analysis of *Dermo1-Cre; R26-loxSTOPlox-YFP* animals between E10.5 and E14.5 revealed evidence of Cre recombination in almost all mesenchymal cells within the cardiac cushions but not in endocardial cells (Figure 3A). Dermo1 Klf2 KO animals survived to birth (Table S1) and exhibited no cushion remodeling defects (Figure 3B), indicating that the defects in Nfatc1 Klf2 KO cardiac cushions arise due to loss of *Klf2* in endocardial and not mesenchymal cells.

To further investigate the endocardial role of *Klf2* specifically during cushion remodeling, we examined mice in which *Klf2* was deleted by an Nfatc1-enhancer Cre transgene that has been reported to be active exclusively in the cushion endocardium following cessation of EMT (Wu et al., 2011; Zhou et al., 2005). Consistent with these studies, R26-loxSTOPlox-YFP (Figure 3C) and R26-loxSTOPlox-LacZ (Figure 3D) reporter analysis demonstrated that the Nfatc1-enhancer Cre transgene drives recombination specifically within the AV and OFT valve endocardium with no detectable mesenchymal cell recombination. However, mice with Nfatc1-enhancer Cre-mediated recombination in cushion endothelial cells (Nfatc1^{en} Klf2 KO mice) were not observed after birth (Table S1), and analysis of E15.5 and E17.5 Nfatc1^{en} Klf2 KO OFT cushions revealed enlarged OFT cushions like those observed in Nfatc1 Klf2 KO animals (Figure 3E). No defects were detected in the AV cushions of Nfatc1^{en} Klf2 KO mice, most likely due to the less penetrant activity of the Nfatc1-enhancer Cre at that site and the fact that the mesenchymal effects of endocardial *Klf2* function are cell non-autonomous. These findings establish that *Klf2* is required specifically in endocardial cells and not in mesenchymal cells for the normal remodeling of cushions to mature valves.

Endocardial Klf2 Regulates Mesenchymal Cell Proliferation and Condensation in the Remodeling Cardiac Cushion

The cellular events associated with cushion remodeling are primarily mesenchymal and include a slowing of mesenchymal proliferation after EMT and the condensation of mesenchymal cells in the region immediately beneath the endocardium to create a thin and mature valve leaflet (Combs and Yutzey, 2009; Kruithof et al., 2007; Person et al., 2005). Analysis of cell proliferation following a bromodeoxyuridine (BrdU) pulse revealed a dramatic decrease in mesenchymal cell proliferation from approximately 40% BrdU+ cells at E11.5 to just over 10% at E14.5 in control cushions (Figures 4A and 4B). Mesenchymal cell proliferation in Nfatc1 Klf2 KO cushions was indistinguishable from that in control cushions at E11.5 but thereafter dropped at approximately half the rate observed in control cushions (Figures 4A and 4B). Endocardial cell proliferation remained unchanged (Figure 4C), and no difference in cellular apoptosis was observed (Figure S3). Notably, the increase in mesenchymal cell proliferation in Nfatc1 Klf2 KO cushions was observed throughout the cushion and not restricted to mesenchymal cells adjacent to the overlying endocardium (Figure 4A).

Mesenchymal cell condensation is a process in which the mesenchymal cells in the region just below the endocardium of the remodeling cushion increase in density (Kruithof et al., 2007). Analysis of H&E- and DAPI-stained sections revealed a significant loss of sub-endocardial mesenchymal cell condensation in Nfatc1 Klf2 KO cushions compared with controls (Figures 4D and 4E). To quantitate mesenchymal cell condensation, we measured the number of mesenchymal cell nuclei within 50, 100. and 150 μm of the endocardial cell layer. At E11.5, there

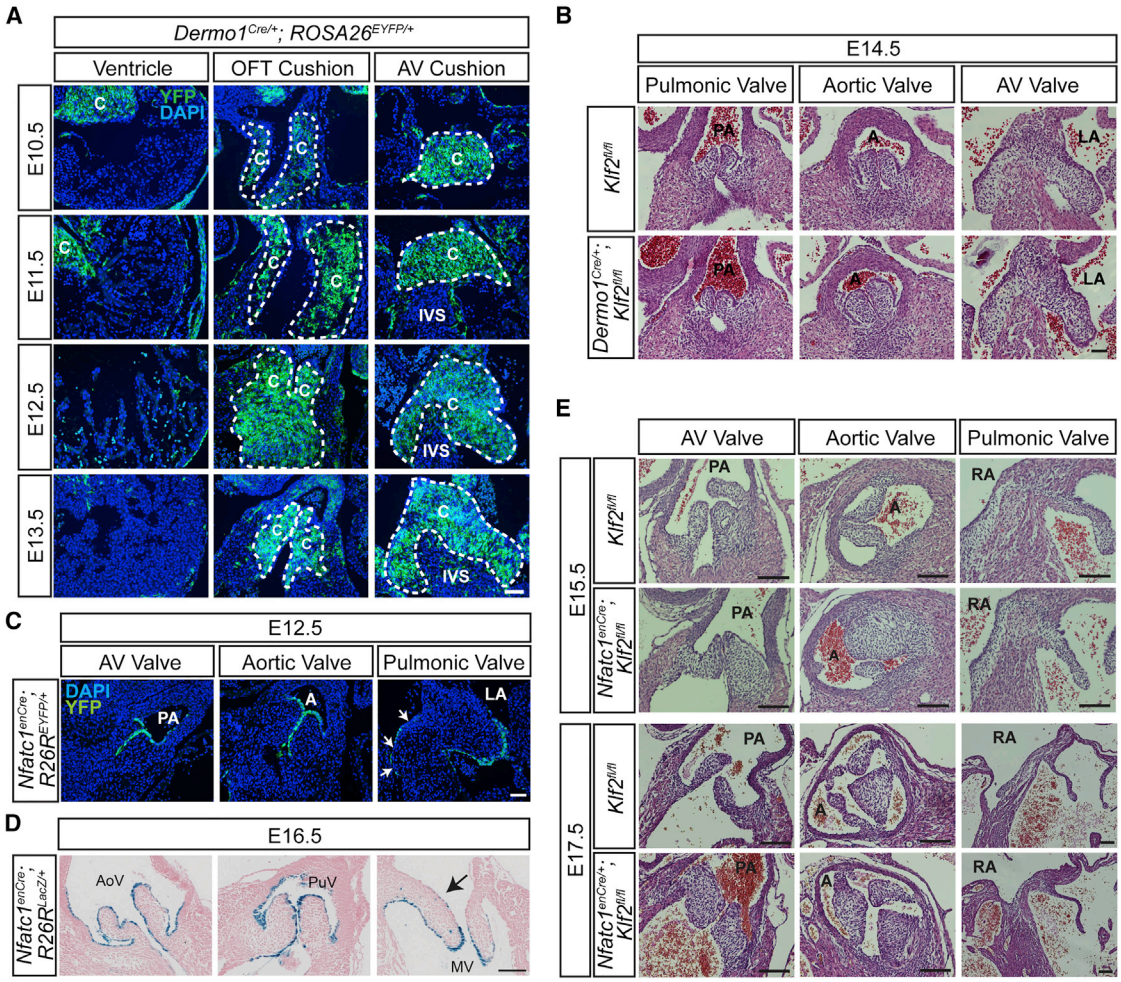

Figure 3. Cushion Mesenchymal Cell Defects following Endocardial *Klf2* Loss Are Cell Non-autonomous

(A) Lineage tracing of Dermo1-Cre; *R26R*^{YFP} cells (green) in the embryonic heart from E10.5 to E13.5. DAPI (blue) stains all nuclei. Scale bar represents 100 μm.

(B) H&E staining of cardiac OFT and AV cushions in *Dermo1*$^{Cre/+}$*; Klf2*$^{fl/fl}$ and littermate control hearts at E14.5. Scale bar represents 100 μm.

(C) Lineage tracing of *Nfatc1*$^{enCre/+}$*; R26R*^{EYFP} mice in the hearts of E12.5 mice. White arrows indicate endocardial cells devoid of reporter activity lining the AV cushion. Scale bar represents 100 μm.

(D) Lineage tracing of *Nfatc1*$^{enCre/+}$*; R26R*^{LacZ} mice in the hearts of E16.5 mice. Black arrows indicate endocardial cells devoid of reporter activity lining the AV valve leaflets. Scale bar represents 100 μm.

(E) H&E staining of OFT and AV valves from E15.5 and E17.5 *Nfatc1*$^{enCre/+}$*;Klf2*$^{fl/fl}$ and littermate controls. Note the enlarged pulmonic and aortic valve cushions compared with controls. Scale bar represents 200 μm.

A, aorta; AoV, aortic valve; C, cushion; IVS, interventricular septum; LA, left atrium; MV, mitral valve; PA, pulmonary artery; PuV, pulmonary valve; RA, right atrium. See also Table S1.

was no appreciable mesenchymal cell condensation in either Nfatc1 Klf2 KO or control cushions (Figure 4F). By E12.5, a significant increase in the density of mesenchymal cell nuclei was evident in the region closest to the endocardium (0–50 μm) of control littermate cushions but not in Nfatc1 Klf2 KO cushions (Figure 4G). By E13.5, a small amount of mesenchymal condensation was observed in Nfatc1 Klf2 KO cushions, but this remained significantly less than that in control littermates (Figures 4D, 4E, and 4H). Similar changes in mesenchymal cell proliferation and condensation were observed in the developing valves of *Nfatc1*$^{Cre/+}$*; Klf2*$^{fl/+}$*; Klf4*$^{fl/fl}$ mice (Figures S2A–S2C). These findings identify persistent mesenchymal cell proliferation and impaired mesenchymal cell condensation as the major cell non-autonomous phenotypes associated with the defective cushion remodeling conferred by loss of endocardial *Klf2* and *Klf4*.

Endocardial Klf2 Deficiency Results in Loss of Endocardial Wnt9b Expression and Reduced Canonical WNT Signaling in Neighboring Mesenchymal Cells

Since KLF2 expression and function are restricted to endocardial cells, the changes in mesenchymal cell proliferation and condensation observed in Nfatc1 Klf2 KO animals must reflect the loss of KLF2-dependent paracrine signals by which the endocardium instructs underlying mesenchymal cells during valve development. To identify such signals, Nfatc1 Klf2 KO

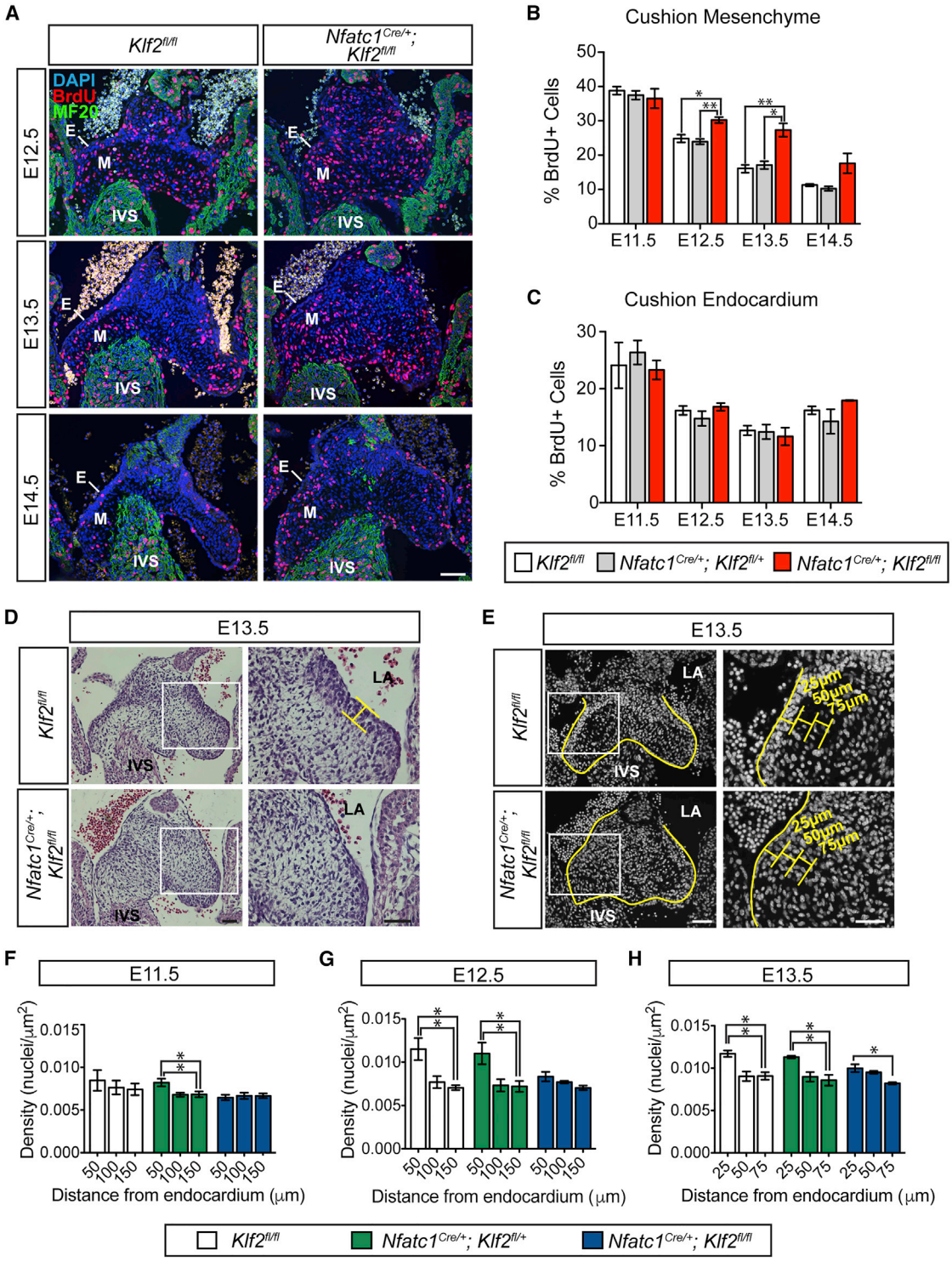

Figure 4. Endocardial Loss of *Klf2* Results in Altered Mesenchymal Cell Proliferation and Condensation in the Cardiac Cushion

(A) Immunostaining to detect BrdU+ cells (red) in *Nfatc1*$^{Cre/+}$*; Klf2*$^{fl/fl}$ and littermate control hearts at E12.5–E14.5. MF20 (green) marks heart muscle and DAPI (blue) denotes cell nuclei.

(B and C) Quantitation of BrdU+ mesenchymal (B) and endocardial (C) cells in the AV cushion of E11.5–E14.5 control and *Nfatc1*$^{Cre/+}$*; Klf2*$^{fl/fl}$ littermates. Error bars represent ±SEM. *p $\leq$ 0.05, **p $\leq$ 0.01 using an unpaired two-tailed Student's t test (n = 3–4 from at least 2 litters).

(D) H&E staining of *Nfatc1*$^{Cre/+}$*; Klf2*$^{fl/fl}$ and control AV cushions at E13.5. High magnification images of the white boxed regions are shown on the right. The bracket indicates the region of mesenchymal cell condensation in control cushions at this time point.

(legend continued on next page)

and littermate control AV cushions were dissected from E12.5 embryos and analyzed by RNA sequencing (RNA-seq) to identify KLF2-regulated genes. Analysis of cushion gene expression revealed a nearly complete loss of *Wnt9b* and markedly reduced levels of the known canonical WNT target genes *Axin2* and *Lef1*, as well as the WNT inhibitory proteins *Notum* and *Apcdd1* (Figures 5A–5C and S5). A complex and dynamic pattern of expression of WNT ligands has been reported in developing heart valves (Alfieri et al., 2010), and reporters have shown abundant canonical WNT activity in the remodeling cushion (Bosada et al., 2016; Gitler et al., 2003) as well as in abluminal cells adjacent to the endothelial cells lining the site of valve development in the zebrafish heart (Pestel et al., 2016), suggesting that WNT signaling may play an important role in this process. However, the precise role played by WNTs in the remodeling of cushions to mature valves and the mechanisms that regulate WNT expression in the remodeling cushion have not been defined.

In situ hybridization studies revealed that *Wnt9b* mRNA expression was restricted to the endocardium with no detectable *Wnt9b* in cushion mesenchymal cells at E12.5 (Figure 5D). As observed for KLF2 and KLF4, *Wnt9b* expression exhibited a graded pattern along the cushion endocardium with peak expression in endothelial cells at the site of close cushion apposition, where shear forces are predicted to be the highest (Figures 5D and 5E). *In situ* hybridization studies confirmed that *Wnt9b* expression was almost abolished in the Nfatc1 Klf2 KO cushion (Figure 5E). To determine whether loss of endocardial KLF2 alters canonical WNT signaling during cushion remodeling, we crossed Nfatc1 Klf2 KO animals onto an $Axin2^{CreERT2-tdTomato}$ reporter in which expression of *Axin2*, a highly characterized and ubiquitous downstream target of canonical WNT signaling (Jho et al., 2002), is marked by expression of the tdTomato protein (Choi et al., 2013). In E12.5 control cushions, canonical WNT signaling was detected exclusively in mesenchymal cells and was notably absent in endocardial cells (Figure 5F). Although canonical WNT signaling was present in both mesenchymal cells adjacent to the endocardium and those deeper within the cushion, it was strongest in the mesenchymal cells adjacent to the endocardium (Figure 5F). Nfatc1 Klf2 KO cushions exhibited a marked reduction of canonical WNT reporter activity throughout the cushion mesenchyme, consistent with endocardial KLF2 regulation of mesenchymal cell WNT signaling (Figure 5F). The persistence of some *Axin2* reporter expression suggests that other signals, derived from either the endocardium or mesenchyme, also regulate canonical WNT signaling in the remodeling cushion.

To test whether KLF2 and/or KLF4 is sufficient to induce expression of *Wnt9b* in endothelial cells, we expressed KLF2, KLF4, or the LacZ gene in human microvascular endothelial cells and measured the expression of *WNT9B* and the known KLF2/4 target gene *NOS3* by qPCR (Figure 5G). Both *WNT9B* and *NOS3* expression were highly induced in response to KLF2 and KLF4 expression (Figure 5G), consistent with a cell autonomous mechanism in which KLF2 and KLF4 drive endocardial expression of *Wnt9b*.

A remarkable finding in our gene expression studies was the lack of any change in *Nfatc1*, a gene expressed by endocardial cells that is known to play a critical role in cushion remodeling similar to that observed for KLF2 (Chang et al., 2004), and a lack of change in expression of *Trpv4*, *Pkd2* (*Trpp2*), or *Fn1* (Figure S5), genes previously associated with *klf2a* function in the developing zebrafish heart valve (Heckel et al., 2015; Steed et al., 2016). To further investigate potential regulation of NFATC1 by KLF2, we stained Nfatc1 Klf2 KO and control cushions with anti-NFATC1 antibodies. Nuclear NFATC1 staining was not reduced in KLF2-deficient endocardial cells of the OFT and AV cushions at E13.5 (Figure S4A), suggesting that the calcineurin/NFATC1 pathway is not downstream of KLF2 during valve development. In addition, overexpression of *NFATC1* in HMVECs did not result in a significant change in *WNT9B* expression (Figure S4B), demonstrating a highly specific regulation of *WNT9B* by KLF2.

Loss of Endocardial Wnt9b Results in Defects in Mesenchymal Cell Proliferation and Condensation Identical to Those Observed with Loss of Endocardial Klf2

The studies described above suggested that loss of canonical WNT signaling in mesenchymal cells is the major molecular abnormality in Nfatc1 Klf2 KO cushions, and that WNT9B might be the endocardial WNT ligand primarily responsible for this defect. WNT9B signaling through both canonical and non-canonical pathways is required for kidney development (Carroll et al., 2005; Karner et al., 2009), but cardiac defects have not been previously described. Analysis of E14.5 embryos from $Wnt9b^{+/-}$ intercrosses generated on a mixed strain background revealed enlarged cardiac cushions in approximately 50% of $Wnt9b^{-/-}$ embryos and septal cushion defects in 100% of $Wnt9b^{-/-}$ embryos, although DORV was not observed (Figures S6A–S6C). Significantly, analysis of cushion mesenchymal cells revealed loss of condensation and increased proliferation like that observed in Nfatc1 Klf2 KO animals (Figures S6D–S6F).

Although our studies (Figures 5D and 5E) and those of others (Alfieri et al., 2010) reveal a highly specific pattern of *Wnt9b* expression in the endocardial cells that overlie the remodeling cardiac cushions, it is possible that global loss of *Wnt9b* alters cushion remodeling indirectly, e.g., through compromised fetal viability or altered hemodynamics associated with renal agenesis or due to an unexpected cell autonomous requirement in mesenchymal cells. To test the role of *Wnt9b* specifically in the heart, we generated Nfatc1 Wnt9b KO and Dermo1 Wnt9b KO animals in which loss of *Wnt9b* is restricted to endocardial cells and endocardial-derived mesenchymal cells or only mesenchymal cells, respectively. The majority of Nfatc1 Wnt9b KO animals died prior to birth (Table S1) and exhibited identical defects in cushion size (Figures 6A and 6B), mesenchymal but not endocardial cell proliferation, and condensation (Figures 6C–6G) to those observed in $Wnt9b^{-/-}$ and Nfatc1

(E) Mesenchymal cell condensation in the indicated AV cushions was calculated by measuring the number of mesenchymal cell nuclei (DAPI, white) per unit area at the indicated distances (yellow brackets) from the endocardium. High magnification images of the white boxed regions are shown on the right.
(F–H) Quantitation of mesenchymal condensation at varying distances from the endocardium in AV cushions from $Nfatc1^{Cre/+}$; $Klf2^{fl/fl}$ and littermate controls at E11.5, E12.5, and E13.5. Error bars represent ±SEM, *$p \leq 0.05$ using an unpaired 2-tailed Student's t test (n = 3 from at least 2 litters).
E, endocardium; IVS, interventricular septum; LA, left atrium; M, mesenchyme. All scale bars represent 100 μm. See also Figures S2 and S3.

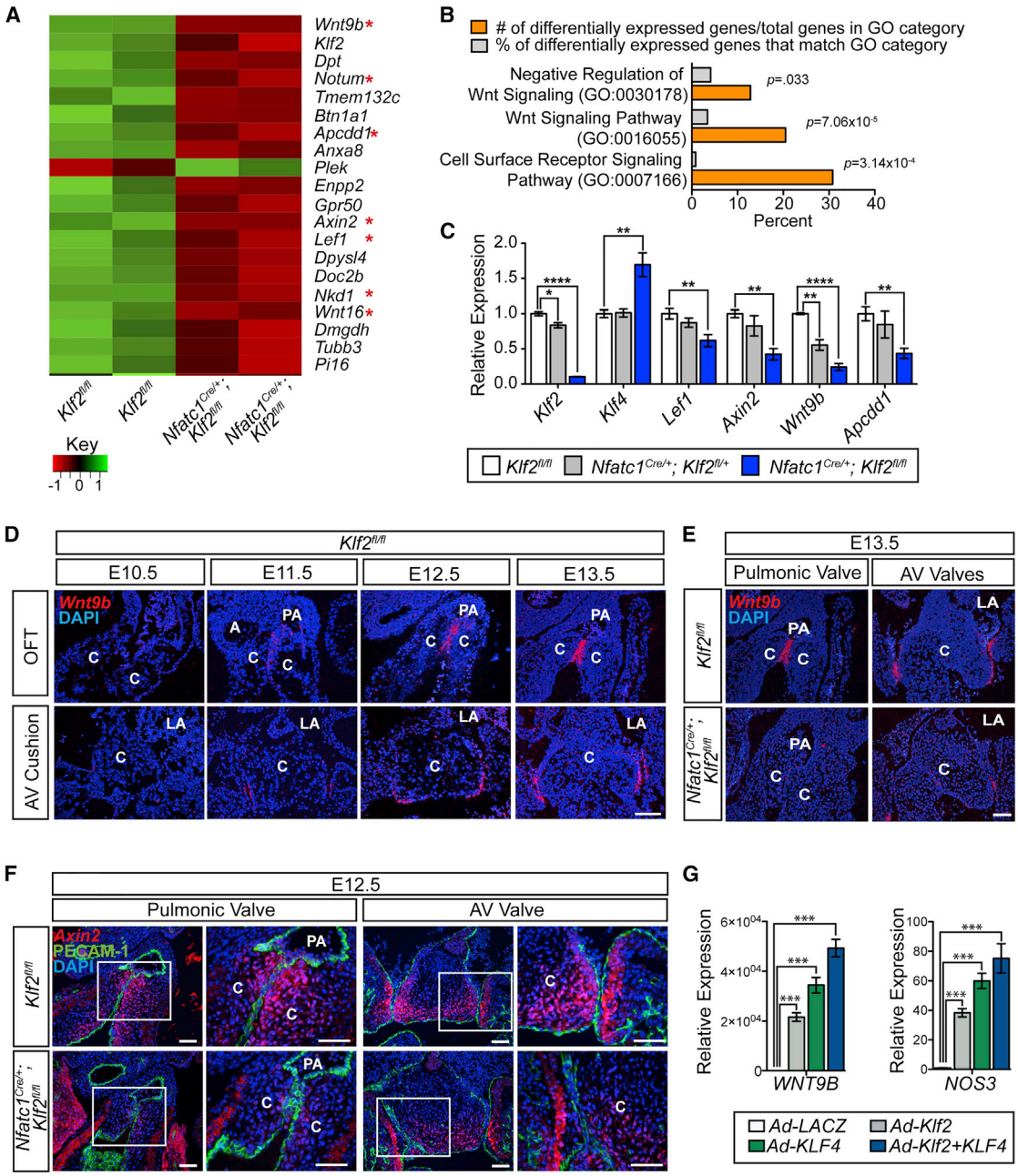

Figure 5. KLF2 Regulates Endocardial *Wnt9b* Expression and Canonical WNT Signaling in Mesenchymal Cells of the Developing Valve

(A) Differential gene expression between E12.5 AV cushions from *Klf2*$^{fl/fl}$ mice and *Nfatc1*$^{Cre/+}$; *Klf2*$^{fl/fl}$ mice was determined using RNA-seq analysis. Heatmap displays the top 20 differentially expressed genes with p $\leq$ 0.05 and false discovery rate $\leq$0.1. Red stars indicate known Wnt signaling genes. Each replicate consists of 6 AV cushions combined from 6 different litters.

(B) Gene ontology analysis of all significant differentially expressed genes between *Klf2*$^{fl/fl}$ and *Nfatc1*$^{Cre/+}$; *Klf2*$^{fl/fl}$ cushions.

(C) qPCR measurement of Wnt target gene expression from the indicated E12.5 hearts. Error bars represent ±SEM, *p $\leq$ 0.05, **p $\leq$ 0.01, ****p $\leq$ 0.0001 using an unpaired two-tailed Student's t test (n = 3–4 from at least 3 litters).

(D) *In situ* hybridization for *Wnt9b* (red) in developing control OFT and AV valves between E10.5 and E13.5. DAPI (blue) staining denotes nuclei. Scale bar represents 100 μm.

(E) *In situ* hybridization for *Wnt9b* (red) in developing *Nfatc1*$^{Cre/+}$; *Klf2*$^{fl/fl}$ and control valves at E13.5. DAPI (blue) staining denotes nuclei. Scale bar represents 100 μm.

(F) *Axin2*$^{CreERT2\text{-}tdTomato}$ reporter activity is detected in the indicated developing heart valves using anti-RFP immunostaining (red). Endocardial cells are identified using anti-PECAM staining (green). High magnification images from boxed regions are shown on the right. Scale bars represent 100μm.

(G) qPCR of *WNT9B* and *NOS3* gene expression in HMVECs following exposure to adenoviral vectors encoding LacZ or KLF2 and/or KLF4 for 24 hr. Error bars represent ±SEM, ***p $\leq$ 0.001 using an unpaired two-tailed Student's t test (n = 3).

A, aorta; C, cushion; LA, left atrium; PA, pulmonary artery. See also Figures S4 and S5.

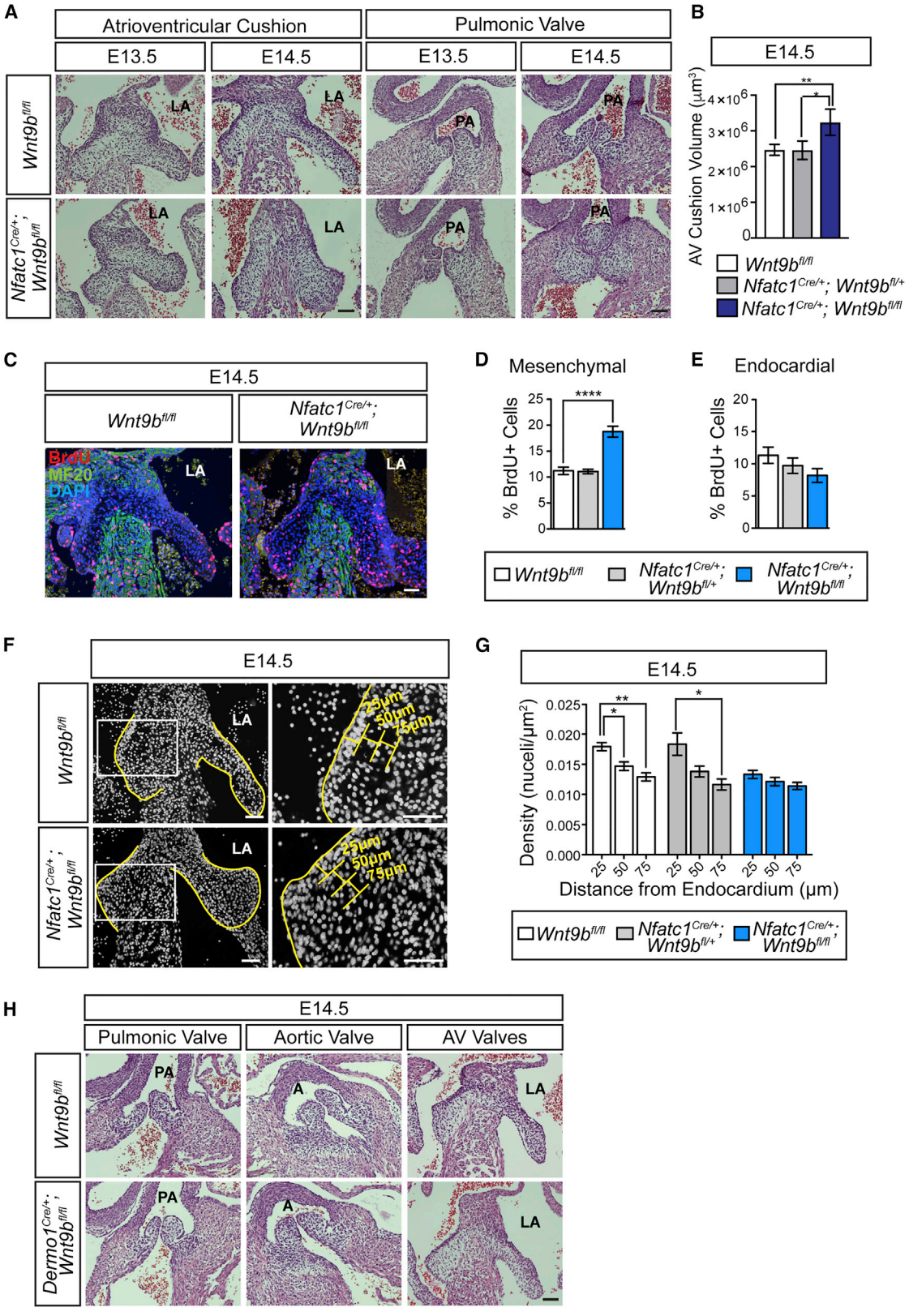

(legend on next page)

Klf2 KO animals. In contrast, Dermo1 Wnt9b KO animals exhibited normal survival and heart valve development (Table S1 and Figure 6H), consistent with an endocardial-specific requirement for *Wnt9b*. Unlike *Wnt9b*$^{-/-}$ animals, the cardiac defects in Nfatc1 Wn9b KO animals were almost fully penetrant, most likely reflecting the effect of background strain, a factor previously reported to influence the phenotype of KLF2-deficient embryos (Chiplunkar et al., 2013). These studies reveal that endocardial KLF2 and WNT9B regulate the same mesenchymal cell responses required for cushion remodeling to mature valves and suggest that KLF2-WNT9B signaling is a primary signaling pathway by which the endocardium regulates heart valve development.

wnt9b Expression Is Endocardial Specific and Regulated by Hemodynamic Forces in the Developing Zebrafish Heart

The studies described above support a model in which hemodynamic forces regulate heart valve development through dynamic endocardial KLF2-WNT9B signaling that instructs underlying mesenchymal cells (Figure S7). However, a direct link between KLF2-WNT9B signaling and hemodynamic forces during this process cannot be tested in the mouse because interruption of blood flow results in lethality prior to cushion remodeling and mature valve formation (Wakimoto et al., 2000). To test the role of hemodynamic forces in this pathway, we next examined the expression of *wnt9b* in zebrafish embryos that are viable without blood flow beyond the time point of heart valve development and in which *klf2a* has been shown to play a requisite role in heart valve development downstream of hemodynamic shear forces (Vermot et al., 2009). Whole-mount *in situ* hybridization for *wnt9b* revealed highly specific expression at the site of the developing AV valve and the outflow tract in the 48 hpf fish heart (Figure 7A), a result that mirrored mouse *Wnt9b* expression (Figures 5D and 5E). To more precisely localize the cellular source of *wnt9b* expression in the developing zebrafish heart, we performed *in situ* hybridization with RNAscope probes that permit simultaneous detection of *wnt9b* and *klf2a* mRNAs on histologic sections (Wang et al., 2012). As previously observed for *klf2a* (Vermot et al., 2009), *wnt9b* was highly specifically expressed in endocardial cells lining the site of the developing AV valve and the cardiac OFT (Figures 7B and 7C). Moreover, confocal analysis demonstrated co-expression of *wnt9b* and *klf2a* by individual endocardial cells at these sites (Figures 7B and 7C). Prior studies have demonstrated that *klf2a* expression in the endocardial cells overlying the developing AV valve is strictly dependent upon blood flow and hemodynamic shear forces (Heckel et al., 2015; Steed et al., 2016; Vermot et al., 2009). As previously shown for *klf2a*, *wnt9b* expression was extinguished or severely reduced in the hearts of *silent heart* (*tnnt2a*) mutant fish that lack blood flow (Sehnert et al., 2002) (Figures 7D and 7E). *wnt9b* expression was also lost in the hearts of *gata1* mutant fish that maintain normal blood flow but experience reduced vascular shear forces due to anemia and low blood viscosity (Figures 7D and 7E). Finally, *wnt9b* expression was markedly reduced in fish hearts lacking *klf2a* (Figures 7D and 7E). These studies reveal a highly specific and conserved pattern of expression for *klf2a* and *wnt9b* in the endocardial cells that overlie the developing heart valve, and establish that endocardial KLF2-WNT9B signaling is strictly regulated by hemodynamic shear forces during heart valve development.

DISCUSSION

Physical forces generated by flowing blood have long been proposed to instruct development of the heart, and of heart valves in particular (Hogers et al., 1999; Hove et al., 2003; Sedmera et al., 1999; Vermot et al., 2009; Yalcin et al., 2010; Steed et al., 2016). However, many of the cellular processes proposed to be regulated by hemodynamic forces during heart valve development take place away from the flowing blood, especially sub-endocardial mesenchymal cell remodeling by which cardiac cushions are remodeled to mature valves. How hemodynamic forces are converted to molecular instructions that are relayed across the endothelium to control such cellular behavior during heart valve development has been unknown. In the present study, we use mouse and zebrafish studies to identify WNT9B as an essential paracrine effector of endocardial KLF2 that is tightly regulated by hemodynamic forces during heart valve development. The KLF2-WNT9B signaling axis is a conserved mechanism by which fluid shear forces experienced by endothelial cells are converted to molecular instructions that direct cells deep within the developing heart valve (Figure S7). These findings reveal a specific molecular mechanism by which cardiovascular forces generated by the beating heart feed back to control its development and suggest that subtle disturbances in this highly precise chain of communication may underlie common valvular congenital defects.

A key link established by these studies is that between the expression of KLF2/4 and WNT9B in the endothelial cells that

Figure 6. Endocardial Loss of *Wnt9b* Confers Valve Defects Like Those Observed with Endocardial Loss of *Klf2*

(A) H&E staining of developing AV and OFT valves in E13.5 and E14.5 *Nfatc1*$^{Cre/+}$*; Wnt9b*$^{fl/fl}$ and control hearts.

(B) Quantitation of AV cushion volumes from *Nfatc1*$^{Cre/+}$*; Wnt9b*$^{fl/fl}$ mice and littermate controls at E14.5. Error bars represent ±SEM, *p ≤ 0.05, **p ≤ 0.01 using an unpaired two-tailed Student's t test (n = 4 from 3 litters).

(C) Immunostaining to detect BrdU+ cells (red) in *Nfatc1*$^{Cre/+}$*; Wnt9b*$^{fl/fl}$ and littermate control hearts at E14.5. MF20 (green) marks heart muscle and DAPI (blue) denotes cell nuclei.

(D and E) Quantitation of BrdU+ mesenchymal (D) and endocardial (E) cells in the AV cushions of E14.5 *Nfatc1*$^{Cre/+}$*; Wnt9b*$^{fl/fl}$ and littermate controls is shown. Error bars represent ±SEM, ****p ≤ 0.0001 using and unpaired two-tailed Student's t test (n = 3–5 from at least 2 litters).

(F) Mesenchymal cell condensation in E14.5 AV cushions was calculated by measuring the number of mesenchymal cell nuclei (DAPI, white) in a given area at indicated distances (yellow brackets) from the endocardium. Images on the right are higher magnification images of the white boxed regions.

(G) Quantitation of mesenchymal condensation at varying distances from the AV cushion endocardium in E14.5 *Nfatc1*$^{Cre/+}$*; Wnt9b*$^{fl/fl}$ hearts compared with littermate controls. Error bars represent ±SEM, *p ≤ 0.05, **p ≤ 0.01 using an unpaired two-tailed Student's t test (n = 3–6 from at least 2 litters).

(H) H&E staining of cardiac OFT and AV cushions in *Dermo1*$^{Cre/+}$*; Wnt9b*$^{fl/fl}$ and littermate control hearts at E14.5.

A, aorta; LA, left atria; PA, pulmonary artery. All scale bars represent 100 μm. See also Figure S6 and Table S1.

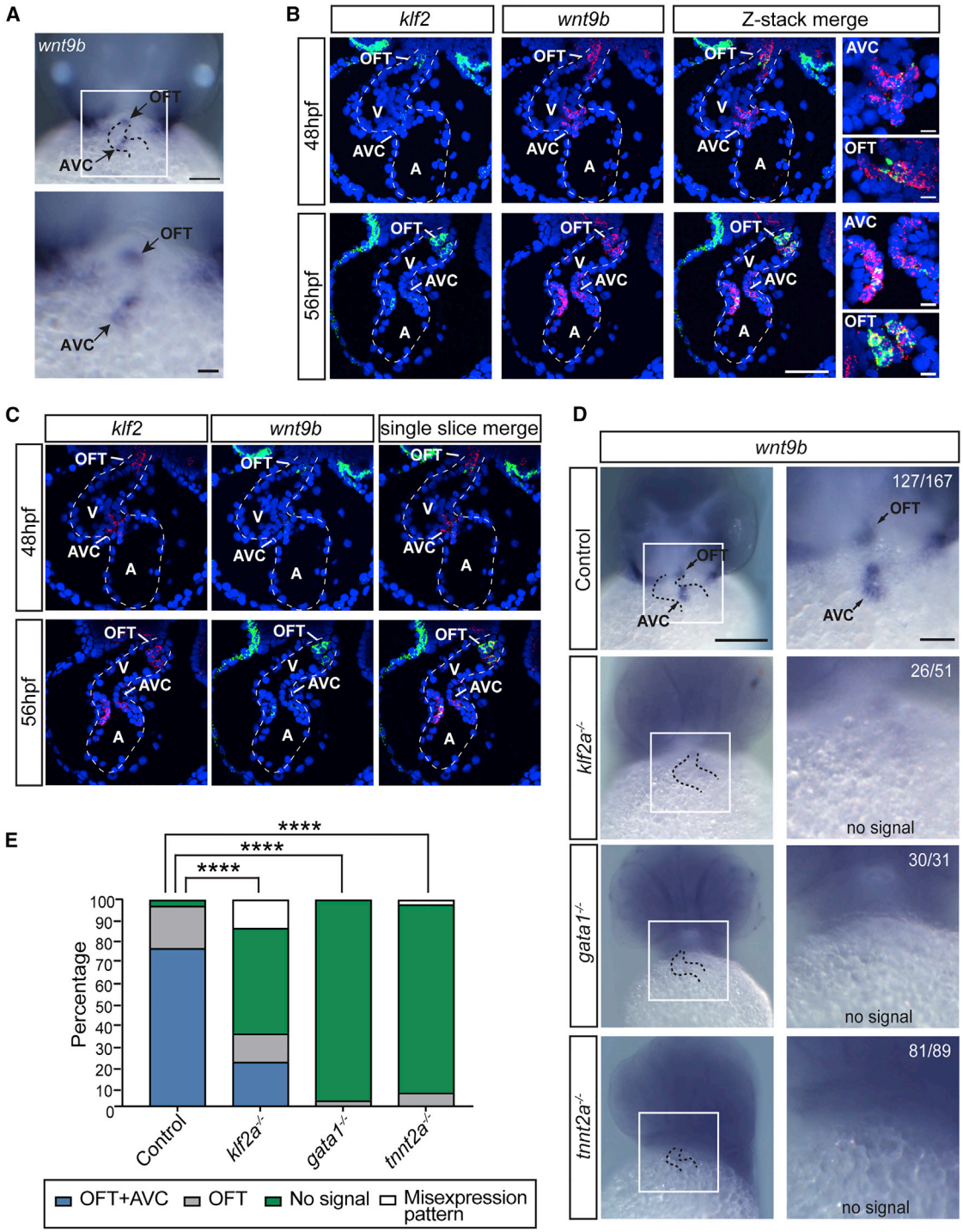

Figure 7. *wnt9b* Expression in the Developing Zebrafish Heart Is Regulated by Hemodynamic Shear Forces

(A) Whole-mount *in situ* hybridization for *wnt9b* in 48 hpf wild-type zebrafish embryos. Dotted lines outline the heart. Scale bars: top, 0.1 mm; bottom, 0.03 mm.

(B and C) *In situ* hybridization using RNAscope for *klf2a* and *wnt9b* in 48 hpf and 56 hpf wild-type zebrafish embryos is shown using merged z stack (B) and single slice (C) confocal analysis. Scale bar represents 100 μm and 10 μm for the magnified images in (B).

(D) *In situ* hybridization to detect *wnt9b* expression in the developing AV cushion and outflow tract of 48 hpf wild-type fish (control), silent heart (*tnnt2a*$^{-/-}$) mutants that lack blood flow, *gata1* mutants (*gata1*$^{-/-}$) that experience low shear stress due to low blood viscosity, and *klf2a* mutants (*klf2a*$^{-/-}$) is shown. Dotted lines outline the heart. Scale bars: left, 0.2 mm; right, 0.06 mm.

(E) The percentage of embryos in which *wnt9b* expression is normal, absent, or mis-expressed in the AV cushion or OFT is shown. The n for each group is indicated in (D). ****$p < 0.0001$ using chi-squared analysis.

A, atrium; AV, atrioventricular; OFT, outflow tract; V, ventricle.

overlie the developing heart valves. Seminal studies in zebrafish embryos have established that heart valves fail to form when blood flow through the heart is mechanically blocked (Hove et al., 2003) and have identified endocardial *klf2a* as a critical effector of fluid shear forces in the developing valve, the expression of which changes rapidly and coordinately with maneuvers that alter hemodynamic forces (Heckel et al., 2015; Renz et al., 2015; Steed et al., 2016; Vermot et al., 2009). These findings are consistent with the identification of *Klf2* as a gene regulated by fluid shear in studies of cultured human endothelial cells (Clark et al., 2011; Dekker et al., 2002; Huddleson et al., 2004; Parmar et al., 2006; Zhou et al., 2015), with the observation that endocardial KLF2 expression is similarly altered by changes in blood flow in the embryonic chicken heart (Groenendijk et al., 2005), with the fact that KLF2 expression in both the mouse and human cardiovascular systems follows predicted shear forces with remarkable cellular resolution (Clark et al., 2011; Dekker et al., 2002; Huddleson et al., 2004; Parmar et al., 2006; Zhou et al., 2015), and with the observation that endocardial KLF2 is expressed in a graded manner predicted by exposure to shear forces in developing valves (Figures 1A–1E) (Lee et al., 2006). Despite this highly conserved association between endothelial KLF2 expression and hemodynamic shear forces, the key effectors of KLF2 have remained obscure and its precise role in coupling fluid shear forces to heart development is unclear. The identification of *Wnt9b* as an essential KLF2 effector downstream of hemodynamic forces in the developing heart valve fills this gap in knowledge and identifies a clear molecular mechanism for the conversion of hemodynamic mechanical forces to biological responses in the heart. Whether hemodynamic forces and KLF2/4 expression are converted to WNT9B signals in particular, or WNT signals in general, at other sites in the cardiovascular system remains an important open question.

The identification of *Wnt9b* as a critical KLF2 effector expressed in response to hemodynamic forces in the developing heart valve is consistent with prior studies of WNT signaling during vertebrate heart valve development and well-established molecular aspects of this signaling mechanism. Canonical WNT signaling has been shown to be required for heart valve development in zebrafish embryos (Hurlstone et al., 2003). More recent studies in the fish have demonstrated that canonical WNT signals arise specifically in sub-endocardial, abluminal cells, a finding analogous to the high level of canonical WNT signaling observed in the sub-endocardial mesenchymal cells of the remodeling cushion in the developing mouse heart (Figure 5F; Gitler et al., 2003), and that these WNT signals are dependent upon hemodynamic forces (Pestel et al., 2016). WNTs are particularly well suited for a role in converting hemodynamic forces sensed by endothelial cells to instructions transmitted to subendothelial cells during this remodeling process because WNT signaling is stringently paracrine (Farin et al., 2016), enabling differences in hemodynamic shear to drive precisely graduated signals at single-cell resolution. A large number of WNT ligands are known to be expressed at distinct time points during heart valve development (Alfieri et al., 2010), but clearly defining the roles of WNT signaling during valve development has been challenging because of potential functional redundancy, the fact that WNT signaling plays numerous roles at distinct times and places (e.g., during EMT and later during cushion remodeling), and that multiple cell types (i.e., myocardial, mesenchymal, endocardial) may secrete and/or respond to WNT ligands (Bosada et al., 2016; Hurlstone et al., 2003; Liebner et al., 2004). Approaches that broadly inhibit canonical WNT signaling (e.g., deletion of β-catenin or overexpression of the canonical pathway inhibitor DKK1; Bosada et al., 2016) have failed to clearly define the roles of WNT signaling in cushion remodeling, because early blockade of WNT signaling inhibits EMT and prevents cushion formation altogether (Hurlstone et al., 2003; Liebner et al., 2004). Our studies reveal that endocardial *Wnt9b* is required to slow mesenchymal cell proliferation and drive the sub-endocardial mesenchymal cell condensation by which a bulky cushion is remodeled into a mature valve cusp. While the effects of *Wnt9b* on sub-endocardial mesenchymal cell condensation are likely to be direct, we also observe changes in mesenchymal cell proliferation deep within the cushion mesenchyme following loss of endocardial *Klf2* or *Wnt9b* that most likely reflect disruption of a still undefined chain of signals initiated by endocardial-mesenchymal cell WNT9B signaling. These studies confirm the proposed complexity of WNT signaling during valve development (Bosada et al., 2016; Gessert and Kuhl, 2010) and highlight the need to study this process in a highly specific spatiotemporal manner.

Our studies support a model in which hemodynamic forces are transduced by endocardial cells through KLF2 and KLF4 that in turn drive paracrine *Wnt9b* signals that provide the primary instructions by which underlying cushion mesenchyme is sculpted to the mature valve (Figure S7). An attractive aspect of this model is that it provides an explanation for how control of heart valve development can be so precisely linked to heart valve function, i.e., how mature valve leaflets can form such that they neither impede the forward flow of blood nor permit its backward flow over a lifetime of constant use. *In vitro* and *in vivo* studies of KLF2 expression in response to fluid shear have revealed robust responses to both pulsatile and reversing flow (Dekker et al., 2002; Heckel et al., 2015; Vermot et al., 2009; Wang et al., 2006). Thus, endocardial cells overlying areas of the remodeling cushion that either excessively oppose forward blood flow or permit backward flow will be subject to higher shear forces and predicted to have higher KLF2/4-WNT9B expression that in turn drives more aggressive underlying cushion remodeling until such stimuli abate. Such a model predicts that even a minor breakdown in the series of precisely graded signals required to accurately transduce such hemodynamic information may result in a subtly defective valve, providing an epigenetic explanation for common congenital valve defects that permit survival to birth. Future studies that more fully define the chain of paracrine signals by which hemodynamic forces direct heart valve development are likely to provide additional insight into why heart defects are the most common congenital abnormality.

STAR★METHODS

Detailed methods are provided in the online version of this paper and include the following:

- KEY RESOURCES TABLE
- CONTACT FOR REAGENT AND RESOURCE SHARING

SUPPLEMENTAL INFORMATION

Supplemental Information includes seven figures, one table, and four movies and can be found with this article online at https://doi.org/10.1016/j.devcel.2017.09.023.

AUTHOR CONTRIBUTIONS

L.M.G. designed and performed most of the experiments and helped write the manuscript. A.L.D. and J.V. designed and performed the zebrafish experiments and helped write the manuscript. M.C., H.R., S.B., D.B.F., B.W., K.A.E., L.L., and J.Y. performed experiments. M.P.M. performed bioinformatics analysis of the RNA-seq dataset. T.W. performed the echocardiographic studies, and M.S.-C. helped interpret the echocardiograph data. S.C.J., E.E.M., and B.Z. contributed essential reagents. T.J.C. contributed essential reagents and helped design the experiments and write the manuscript. M.L.K. helped design the experiments and write the manuscript.

ACKNOWLEDGMENTS

The authors thank members of the Kahn lab and the Sarah Millar lab for discussion and insight during the process of this work. These studies were supported by NIH grants R01HL094326 (M.L.K.), T32HL007954 (L.M.G.), and R0111770 and R01116997 (B.Z). J.V. and A.L.D. are supported by the Agence Nationale de la Recherche (ANR) (ANR-15-CE13-0015-01). J.V. is supported by a European Research Council consolidator grant Evalve (682938), Fondation pour la Recherche Médicale (DEQ20140329553), and grant ANR-10-LABX-0030-INRT, a French State fund managed by the ANR under the frame program Investissements d'Avenir labeled ANR-10-IDEX-0002-02.

Received: July 23, 2016
Revised: August 1, 2017
Accepted: September 25, 2017
Published: October 19, 2017

REFERENCES

Alfieri, C.M., Cheek, J., Chakraborty, S., and Yutzey, K.E. (2010). Wnt signaling in heart valve development and osteogenic gene induction. Dev. Biol. *338*, 127–135.

Ashburner, M., Ball, C.A., Blake, J.A., Botstein, D., Butler, H., Cherry, J.M., Davis, A.P., Dolinski, K., Dwight, S.S., Eppig, J.T., et al. (2000). Gene ontology: tool for the unification of biology. The Gene Ontology Consortium. Nat. Genet. *25*, 25–29.

Bosada, F.M., Devasthali, V., Jones, K.A., and Stankunas, K. (2016). Wnt/beta-catenin signaling enables developmental transitions during valvulogenesis. Development *143*, 1041–1054.

Carroll, T.J., Park, J.S., Hayashi, S., Majumdar, A., and McMahon, A.P. (2005). Wnt9b plays a central role in the regulation of mesenchymal to epithelial transitions underlying organogenesis of the mammalian urogenital system. Dev. Cell *9*, 283–292.

Chang, C.P., Neilson, J.R., Bayle, J.H., Gestwicki, J.E., Kuo, A., Stankunas, K., Graef, I.A., and Crabtree, G.R. (2004). A field of myocardial-endocardial NFAT signaling underlies heart valve morphogenesis. Cell *118*, 649–663.

Chiplunkar, A.R., Lung, T.K., Alhashem, Y., Koppenhaver, B.A., Salloum, F.N., Kukreja, R.C., Haar, J.L., and Lloyd, J.A. (2013). Kruppel-like factor 2 is required for normal mouse cardiac development. PLoS One *8*, e54891.

Choi, Y.S., Zhang, Y., Xu, M., Yang, Y., Ito, M., Peng, T., Cui, Z., Nagy, A., Hadjantonakis, A.K., Lang, R.A., et al. (2013). Distinct functions for Wnt/beta-catenin in hair follicle stem cell proliferation and survival and interfollicular epidermal homeostasis. Cell Stem Cell *13*, 720–733.

Clark, P.R., Jensen, T.J., Kluger, M.S., Morelock, M., Hanidu, A., Qi, Z., Tatake, R.J., and Pober, J.S. (2011). MEK5 is activated by shear stress, activates ERK5 and induces KLF4 to modulate TNF responses in human dermal microvascular endothelial cells. Microcirculation *18*, 102–117.

Combs, M.D., and Yutzey, K.E. (2009). Heart valve development: regulatory networks in development and disease. Circ. Res. *105*, 408–421.

Dekker, R.J., van Soest, S., Fontijn, R.D., Salamanca, S., de Groot, P.G., VanBavel, E., Pannekoek, H., and Horrevoets, A.J. (2002). Prolonged fluid shear stress induces a distinct set of endothelial cell genes, most specifically lung Kruppel-like factor (KLF2). Blood *100*, 1689–1698.

Dekker, R.J., van Thienen, J.V., Rohlena, J., de Jager, S.C., Elderkamp, Y.W., Seppen, J., de Vries, C.J., Biessen, E.A., van Berkel, T.J., Pannekoek, H., et al. (2005). Endothelial KLF2 links local arterial shear stress levels to the expression of vascular tone-regulating genes. Am. J. Pathol. *167*, 609–618.

Dina, C., Bouatia-Naji, N., Tucker, N., Delling, F.N., Toomer, K., Durst, R., Perrocheau, M., Fernandez-Friera, L., Solis, J., investigators, P., et al. (2015). Genetic association analyses highlight biological pathways underlying mitral valve prolapse. Nat. Genet. *47*, 1206–1211.

Durst, R., Sauls, K., Peal, D.S., deVlaming, A., Toomer, K., Leyne, M., Salani, M., Talkowski, M.E., Brand, H., Perrocheau, M., et al. (2015). Mutations in DCHS1 cause mitral valve prolapse. Nature *525*, 109–113.

Farin, H.F., Jordens, I., Mosa, M.H., Basak, O., Korving, J., Tauriello, D.V., de Punder, K., Angers, S., Peters, P.J., Maurice, M.M., et al. (2016). Visualization of a short-range Wnt gradient in the intestinal stem-cell niche. Nature *530*, 340–343.

Garg, V., Muth, A.N., Ransom, J.F., Schluterman, M.K., Barnes, R., King, I.N., Grossfeld, P.D., and Srivastava, D. (2005). Mutations in NOTCH1 cause aortic valve disease. Nature *437*, 270–274.

Gene Ontology Consortium. (2015). Gene ontology consortium: going forward. Nucleic Acids Res. *43*, D1049–D1056.

Gessert, S., and Kuhl, M. (2010). The multiple phases and faces of wnt signaling during cardiac differentiation and development. Circ. Res. *107*, 186–199.

Gitler, A.D., Lu, M.M., Jiang, Y.Q., Epstein, J.A., and Gruber, P.J. (2003). Molecular markers of cardiac endocardial cushion development. Dev. Dyn. *228*, 643–650.

Groenendijk, B.C., Hierck, B.P., Vrolijk, J., Baiker, M., Pourquie, M.J., Gittenberger-de Groot, A.C., and Poelmann, R.E. (2005). Changes in shear stress-related gene expression after experimentally altered venous return in the chicken embryo. Circ. Res. *96*, 1291–1298.

Heckel, E., Boselli, F., Roth, S., Krudewig, A., Belting, H.G., Charvin, G., and Vermot, J. (2015). Oscillatory flow modulates mechanosensitive klf2a expression through trpv4 and trpp2 during heart valve development. Curr. Biol. *25*, 1354–1361.

Hoffman, J.I., and Kaplan, S. (2002). The incidence of congenital heart disease. J. Am. Coll. Cardiol. *39*, 1890–1900.

Hogers, B., DeRuiter, M.C., Gittenberger-de Groot, A.C., and Poelmann, R.E. (1999). Extraembryonic venous obstructions lead to cardiovascular malformations and can be embryo lethal. Cardiovasc. Res. *41*, 87–99.

Hove, J.R., Koster, R.W., Forouhar, A.S., Acevedo-Bolton, G., Fraser, S.E., and Gharib, M. (2003). Intracardiac fluid forces are an essential epigenetic factor for embryonic cardiogenesis. Nature *421*, 172–177.

Huddleson, J.P., Srinivasan, S., Ahmad, N., and Lingrel, J.B. (2004). Fluid shear stress induces endothelial KLF2 gene expression through a defined promoter region. Biol. Chem. *385*, 723–729.

Hurlstone, A.F., Haramis, A.P., Wienholds, E., Begthel, H., Korving, J., Van Eeden, F., Cuppen, E., Zivkovic, D., Plasterk, R.H., and Clevers, H. (2003). The Wnt/beta-catenin pathway regulates cardiac valve formation. Nature *425*, 633–637.

Jaffee, O.C. (1965). Hemodynamic factors in the development of the chick embryo heart. Anat. Rec. *151*, 69–75.

Jho, E.H., Zhang, T., Domon, C., Joo, C.K., Freund, J.N., and Costantini, F. (2002). Wnt/beta-catenin/Tcf signaling induces the transcription of Axin2, a negative regulator of the signaling pathway. Mol. Cell. Biol. *22*, 1172–1183.

Karner, C.M., Chirumamilla, R., Aoki, S., Igarashi, P., Wallingford, J.B., and Carroll, T.J. (2009). Wnt9b signaling regulates planar cell polarity and kidney tubule morphogenesis. Nat. Genet. *41*, 793–799.

Katz, J.P., Perreault, N., Goldstein, B.G., Lee, C.S., Labosky, P.A., Yang, V.W., and Kaestner, K.H. (2002). The zinc-finger transcription factor Klf4 is required for terminal differentiation of goblet cells in the colon. Development *129*, 2619–2628.

Kruithof, B.P., Krawitz, S.A., and Gaussin, V. (2007). Atrioventricular valve development during late embryonic and postnatal stages involves condensation and extracellular matrix remodeling. Dev. Biol. *302*, 208–217.

Langmead, B., and Salzberg, S.L. (2012). Fast gapped-read alignment with Bowtie 2. Nat. Methods *9*, 357–359.

Lee, J.S., Yu, Q., Shin, J.T., Sebzda, E., Bertozzi, C., Chen, M., Mericko, P., Stadtfeld, M., Zhou, D., Cheng, L., et al. (2006). Klf2 is an essential regulator of vascular hemodynamic forces in vivo. Dev. Cell *11*, 845–857.

Levine, R.A., Hagege, A.A., Judge, D.P., Padala, M., Dal-Bianco, J.P., Aikawa, E., Beaudoin, J., Bischoff, J., Bouatia-Naji, N., Bruneval, P., et al. (2015). Mitral valve disease–morphology and mechanisms. Nat. Rev. Cardiol. *12*, 689–710.

Liebner, S., Cattelino, A., Gallini, R., Rudini, N., Iurlaro, M., Piccolo, S., and Dejana, E. (2004). Beta-catenin is required for endothelial-mesenchymal transformation during heart cushion development in the mouse. J. Cell Biol. *166*, 359–367.

Lin, C.J., Lin, C.Y., Chen, C.H., Zhou, B., and Chang, C.P. (2012). Partitioning the heart: mechanisms of cardiac septation and valve development. Development *139*, 3277–3299.

Lin, W., Seidler, F.J., McCook, E.C., and Slotkin, T.A. (1992). Overexpression of alpha 2-adrenergic receptors in fetal rat heart: receptors in search of a function. J. Dev. Physiol. *17*, 183–187.

Lyons, S.E., Lawson, N.D., Lei, L., Bennett, P.E., Weinstein, B.M., and Liu, P.P. (2002). A nonsense mutation in zebrafish gata1 causes the bloodless phenotype in vlad tepes. Proc. Natl. Acad. Sci. USA *99*, 5454–5459.

MacGrogan, D., Luxan, G., Driessen-Mol, A., Bouten, C., Baaijens, F., and de la Pompa, J.L. (2014). How to make a heart valve: from embryonic development to bioengineering of living valve substitutes. Cold Spring Harb. Perspect. Med. *4*, a013912.

Madisen, L., Zwingman, T.A., Sunkin, S.M., Oh, S.W., Zariwala, H.A., Gu, H., Ng, L.L., Palmiter, R.D., Hawrylycz, M.J., Jones, A.R., et al. (2010). A robust and high-throughput Cre reporting and characterization system for the whole mouse brain. Nat. Neurosci. *13*, 133–140.

Markwald, R.R., Fitzharris, T.P., and Manasek, F.J. (1977). Structural development of endocardial cushions. Am. J. Anat. *148*, 85–119.

McCarthy, D.J., Chen, Y., and Smyth, G.K. (2012). Differential expression analysis of multifactor RNA-Seq experiments with respect to biological variation. Nucleic Acids Res. *40*, 4288–4297.

McCormick, S.M., Eskin, S.G., McIntire, L.V., Teng, C.L., Lu, C.M., Russell, C.G., and Chittur, K.K. (2001). DNA microarray reveals changes in gene expression of shear stressed human umbilical vein endothelial cells. Proc. Natl. Acad. Sci. USA *98*, 8955–8960.

Parmar, K.M., Larman, H.B., Dai, G., Zhang, Y., Wang, E.T., Moorthy, S.N., Kratz, J.R., Lin, Z., Jain, M.K., Gimbrone, M.A., et al. (2006). Integration of flow-dependent endothelial phenotypes by Kruppel-like factor 2. J. Clin. Invest. *116*, 49–58.

Parmar, K.M., Nambudiri, V., Dai, G., Larman, H.B., Gimbrone, M.A., Jr., and Garcia-Cardena, G. (2005). Statins exert endothelial atheroprotective effects via the KLF2 transcription factor. J. Biol. Chem. *280*, 26714–26719.

Person, A.D., Klewer, S.E., and Runyan, R.B. (2005). Cell biology of cardiac cushion development. Int. Rev. Cytol. *243*, 287–335.

Pestel, J., Ramadass, R., Gauvrit, S., Helker, C., Herzog, W., and Stainier, D.Y. (2016). Real-time 3D visualization of cellular rearrangements during cardiac valve formation. Development *143*, 2217–2227.

Renz, M., Otten, C., Faurobert, E., Rudolph, F., Zhu, Y., Boulday, G., Duchene, J., Mickoleit, M., Dietrich, A.C., Ramspacher, C., et al. (2015). Regulation of beta1 integrin-Klf2-mediated angiogenesis by CCM proteins. Dev. Cell *32*, 181–190.

Richards, A.A., and Garg, V. (2010). Genetics of congenital heart disease. Curr. Cardiol. Rev. *6*, 91–97.

Robinson, M.D., McCarthy, D.J., and Smyth, G.K. (2010). edgeR: a Bioconductor package for differential expression analysis of digital gene expression data. Bioinformatics *26*, 139–140.

Sedmera, D., Pexieder, T., Rychterova, V., Hu, N., and Clark, E.B. (1999). Remodeling of chick embryonic ventricular myoarchitecture under experimentally changed loading conditions. Anat. Rec. *254*, 238–252.

Segre, J.A., Bauer, C., and Fuchs, E. (1999). Klf4 is a transcription factor required for establishing the barrier function of the skin. Nat. Genet. *22*, 356–360.

Sehnert, A.J., Huq, A., Weinstein, B.M., Walker, C., Fishman, M., and Stainier, D.Y. (2002). Cardiac troponin T is essential in sarcomere assembly and cardiac contractility. Nat. Genet. *31*, 106–110.

Sharpe, J., Ahlgren, U., Perry, P., Hill, B., Ross, A., Hecksher-Sorensen, J., Baldock, R., and Davidson, D. (2002). Optical projection tomography as a tool for 3D microscopy and gene expression studies. Science *296*, 541–545.

Sosic, D., Richardson, J.A., Yu, K., Ornitz, D.M., and Olson, E.N. (2003). Twist regulates cytokine gene expression through a negative feedback loop that represses NF-kappaB activity. Cell *112*, 169–180.

Steed, E., Faggianelli, N., Roth, S., Ramspacher, C., Concordet, J.P., and Vermot, J. (2016). klf2a couples mechanotransduction and zebrafish valve morphogenesis through fibronectin synthesis. Nat. Commun. *7*, 11646.

Theodoris, C.V., Li, M., White, M.P., Liu, L., He, D., Pollard, K.S., Bruneau, B.G., and Srivastava, D. (2015). Human disease modeling reveals integrated transcriptional and epigenetic mechanisms of NOTCH1 haploinsufficiency. Cell *160*, 1072–1086.

Thisse, C., and Thisse, B. (2008). High-resolution in situ hybridization to whole-mount zebrafish embryos. Nat. Protoc. *3*, 59–69.

Vermot, J., Forouhar, A.S., Liebling, M., Wu, D., Plummer, D., Gharib, M., and Fraser, S.E. (2009). Reversing blood flows act through klf2a to ensure normal valvulogenesis in the developing heart. PLoS Biol. *7*, e1000246.

von Gise, A., and Pu, W.T. (2012). Endocardial and epicardial epithelial to mesenchymal transitions in heart development and disease. Circ. Res. *110*, 1628–1645.

Wakimoto, K., Kobayashi, K., Kuro, O.M., Yao, A., Iwamoto, T., Yanaka, N., Kita, S., Nishida, A., Azuma, S., Toyoda, Y., et al. (2000). Targeted disruption of Na+/Ca2+ exchanger gene leads to cardiomyocyte apoptosis and defects in heartbeat. J. Biol. Chem. *275*, 36991–36998.

Wang, F., Flanagan, J., Su, N., Wang, L.C., Bui, S., Nielson, A., Wu, X., Vo, H.T., Ma, X.J., and Luo, Y. (2012). RNAscope: a novel in situ RNA analysis platform for formalin-fixed, paraffin-embedded tissues. J. Mol. Diagn. *14*, 22–29.

Wang, N., Miao, H., Li, Y.S., Zhang, P., Haga, J.H., Hu, Y., Young, A., Yuan, S., Nguyen, P., Wu, C.C., et al. (2006). Shear stress regulation of Kruppel-like factor 2 expression is flow pattern-specific. Biochem. Biophys. Res. Commun. *341*, 1244–1251.

Weinreich, M.A., Takada, K., Skon, C., Reiner, S.L., Jameson, S.C., and Hogquist, K.A. (2009). KLF2 transcription-factor deficiency in T cells results in unrestrained cytokine production and upregulation of bystander chemokine receptors. Immunity *31*, 122–130.

Wu, B., Wang, Y., Lui, W., Langworthy, M., Tompkins, K.L., Hatzopoulos, A.K., Baldwin, H.S., and Zhou, B. (2011). Nfatc1 coordinates valve endocardial cell lineage development required for heart valve formation. Circ. Res. *109*, 183–192.

Wu, B., Zhang, Z., Lui, W., Chen, X., Wang, Y., Chamberlain, A.A., Moreno-Rodriguez, R.A., Markwald, R.R., O'Rourke, B.P., Sharp, D.J., et al. (2012). Endocardial cells form the coronary arteries by angiogenesis through myocardial-endocardial VEGF signaling. Cell *151*, 1083–1096.

Yalcin, H.C., Shekhar, A., Nishimura, N., Rane, A.A., Schaffer, C.B., and Butcher, J.T. (2010). Two-photon microscopy-guided femtosecond-laser photoablation of avian cardiogenesis: noninvasive creation of localized heart defects. Am. J. Physiol. Heart Circ. Physiol. *299*, H1728–H1735.

Zhou, B., Wu, B., Tompkins, K.L., Boyer, K.L., Grindley, J.C., and Baldwin, H.S. (2005). Characterization of Nfatc1 regulation identifies an enhancer required for gene expression that is specific to pro-valve endocardial cells in the developing heart. Development *132*, 1137–1146.

Zhou, Z., Rawnsley, D.R., Goddard, L.M., Pan, W., Cao, X.J., Jakus, Z., Zheng, H., Yang, J., Arthur, J.S., Whitehead, K.J., et al. (2015). The cerebral cavernous malformation pathway controls cardiac development via regulation of endocardial MEKK3 signaling and KLF expression. Dev. Cell *32*, 168–180.

STAR★METHODS

KEY RESOURCES TABLE

REAGENT or RESOURCE	SOURCE	IDENTIFIER
Antibodies		
Goat anti-GFP	Abcam	CAT#ab6673; RRID: AB_305643
Rat anti-BrdU	Abcam	CAT#ab6326; RRID: AB_305426
Mouse anti-MF20	Developmental Studies Hybridoma Bank	RRID: AB_2147781
Rabbit anti-RFP	Rockland	CAT# 600-401-379; RRID:AB_2209751
Goat anti-KLF4	R&D Systems	CAT# AF3158; RRID:AB_2130245
Rat anti-PECAM-1	Dianova	CAT# DIA-310; RRID:AB_2631039
Mouse anti-FIBRONECTIN (EP5)	Santa Cruz Biotechnology	CAT# sc-8422; RRID:AB_627598
Mouse anti-NF-ATc1	BD Biosciences	CAT# 556602; RRID:AB_396478
Bacterial and Virus Strains		
Ad-h-NFATC1 Human adenovirus Type 5 (dE1/E3)	Vector Biolabs	CAT#ADV-216628
Ad-h-KLF4 Human adenovirus Type 5 (dE1/E3)	Vector Biolabs	CAT#1787
H5.040CMV_mHAKLF2	Penn Vector Core	N/A
H5.040CMV_LacZ	Penn Vector Core	N/A
Chemicals, Peptides, and Recombinant Proteins		
Power SYBR Green PCR Master Mix	ThermoFIsher	CAT# 4368708
5-Bromo-2′-deoxyuridine BioUltra ≥99% (BrdU)	Sigma	CAT# B9285
EGM2-MV Bullet Kit	Lonza	CAT# CC-3202
TRIzol	Invitrogen	CAT# 15596026
RNAlater RNA Stabilization Reagent	QIAGEN	CAT# 76104
Proteinase K	Sigma	CAT# P2308
Tween-20	Sigma	CAT# P9416
Blocking reagent	Roche	CAT# 11096176001
BM-purple	Sigma	CAT# 11442074001
Anti-Digoxigenin-AP, Fab fragments from sheep	Roche	CAT# 11093274910
tRNA	Roche	CAT# 10109517001
Critical Commercial Assays		
QIAGEN RNeasy Mini kit	QIAGEN	CAT# 74134
QIAGEN RNeasy Micro kit	QIAGEN	CAT#74034
TruSeq Stranded Total RNA Library Prep Kit	Illumina	CAT# RS-122-2201
Superscript III First Strand Synthesis System	ThermoFisher	CAT# 18080051
RNAscope Multiplex Fluorescent v2	ACD	CAT# 323110
mMESSAGE mMACHINE SP6 Transcription Kit	ThermoFisher	CAT# AM1340
Deposited Data		
Raw RNA-Seq data set	This paper	GEO: GSE80964
Experimental Models: Cell Lines		
Human Dermal Microvascular Lymphatic Endothelial Cells,HMVEC-dLy	Lonza	CAT# CC-2812
Experimental Models: Organisms/Strains		
Mouse: *Nfatc1*^{Cre}	Wu et al., 2012	N/A
Mouse: *Nfatc1*^{enCre}	Wu et al., 2011	N/A
Mouse: *Klf2*$^{fl/fl}$	Lee et al., 2006	N/A
Mouse: *Klf2*^{GFP}	Weinreich et al., 2009	N/A

(*Continued on next page*)

Continued

REAGENT or RESOURCE	SOURCE	IDENTIFIER
Mouse: *Axin2*$^{CreERT2/tdT}$	Choi et al., 2013	N/A
Mouse: *Wnt9b*$^{-/-}$	Carroll et al., 2005	N/A
Mouse: *Wnt9b*$^{fl/fl}$	Carroll et al., 2005	N/A
Mouse: *Klf4*$^{fl/fl}$	Katz et al., 2002	N/A
Mouse: *Rosa*^{EYFP}	Madisen et al., 2010	N/A
Mouse: *Dermo1*^{Cre}	Sosic et al., 2003	N/A
Zebrafish: *Tg(klf2a*^{ig4}*)*	Steed et al., 2016	N/A
Zebrafish: *vlad tepes*^{m651} (*gata1*)	Lyons et al., 2002	N/A
Zebrafish: *tnnt2a*^{tc300b}	Sehnert et al., 2002	N/A
Oligonucleotides		
hWNT9B qPCR primers: F: 5'CAGCACCAAGTTTCTGAGCA3' R: 5'CCGAGTCATAGCGCAGTTTC3'	Integrated DNA Technologies	N/A
hNOS3 qPCR primers: F: 5'GGGTCCTGTGTATGGATGAGT3' R: 5'ATGCTGTTGAAGCGGATCTTA3'	Integrated DNA Technologies	N/A
hNFATC1 qPCR primers: F: 5'GGAAGGGCGGCTTCTGCGAC3' R: 5'AGGCGTGCGGGCGCAGCAG3'	Integrated DNA Technologies	N/A
mKlf2 qPCR primers: F: 5'CGCCTCGGGTTCATTTC3' R: 5'AGCCTATCTTGCCGTCCTTT3'	Integrated DNA Technologies	N/A
mKlf4 qPCR primers: F: 5'GTGCCCCGACTAACCGTTG3' R: 5'GTCGTTGAACTCCTCGGTCT3'	Integrated DNA Technologies	N/A
mAxin2 qPCR primers: F: 5'CAGCCCTTGTGGTTCAAGCT3' R: 5'GGTAGATTCCTGATGGCCGATGT3'	Integrated DNA Technologies	N/A
mLef1 qPCR primers: F: 5'TAACGAGTCCGAAATCATCCCAGC3' R: 5'TTCATCAGGGTGTTCTCTGGCCTT3'	Integrated DNA Technologies	N/A
mApcdd1 qPCR primers: F: 5'AGAAGCAGTATCCCCACCAC3' R: 5'CAGTATGGGAGGGTGGTGTT3'	Integrated DNA Technologies	N/A
mWnt9b qPCR primers: F: 5'TGTCAGTTCCAGTTCAGGCA3' R: 5'GGGGAGTCGTCACAAGTACA3'	Integrated DNA Technologies	N/A
mWnt16 qPCR primers: F: 5'AACTGGATGTGGTTGGGCAT3' R: 5'ACCTCTCGTGTCGGAACTG3'	Integrated DNA Technologies	N/A
mFn1 qPCR primers: F: 5'TCCGAGAGATCTGGAGGTCA3' R: 5'GGTGTAGTCTGCTCCTGGTT3'	Integrated DNA Technologies	N/A
mWnt4 qPCR primers: F: 5'AACTGCTCCACACTCGACTC3' R: 5'CCATGCACTGTCCTGTCACA3'	Integrated DNA Technologies	N/A
mWnt11 qPCR primers: F: 5'GATATCCGGCCTGTGAAGGA3' R: 5'CCGTTGGAAGTCTTGTTGCA3'	Integrated DNA Technologies	N/A
mPkd2 qPCR primers: F: 5'TACGGCATGATGAGCTCCAA3' R: 5'CTGGTCTGTGCCTTCCAGTA3'	Integrated DNA Technologies	N/A
mTrpv4 qPCR primers: F: 5'TTCAAGGACTGGGCCTATGG3' R: 5'GACACAGCCCCAAACTTACG3'	Integrated DNA Technologies	N/A

(*Continued on next page*)

Continued

REAGENT or RESOURCE	SOURCE	IDENTIFIER
Software and Algorithms		
Casava1.8.2	Illumina	N/A
Gene Ontology (Biological Processes) Analysis	Gene Ontology Consortium	http://www.geneontology.org/
Bowtie version 0.12.7	Langmead and Salzberg, 2012	https://sourceforge.net/projects/bowtie-bio/files/bowtie/0.12.7/
EdgeR software	Robinson et al., 2010; McCarthy et al., 2012	https://bioconductor.org/packages/release/bioc/html/edgeR.html
Prism	GraphPad	https://www.graphpad.com/scientific-software/prism/
ImageJ	NIH	https://imagej.nih.gov/ij/

CONTACT FOR REAGENT AND RESOURCE SHARING

Further information and requests for resources and reagents should be directed to and will be fulfilled by the Lead Contact, Mark Kahn (markkahn@pennmedicine.upenn.edu).

EXPERIMENTAL MODEL AND SUBJECT DETAILS

Mouse Models

Nfatc1^{Cre} (Wu et al., 2012), *Nfatc1*^{enCre} (Wu et al., 2011), *Klf2*$^{fl/fl}$ (Lee et al., 2006), *Klf2*^{GFP} (Weinreich et al., 2009), *Axin2*$^{CreERT2/tdT}$ (Choi et al., 2013), *Wnt9b*$^{-/-}$ (Carroll et al., 2005), *Wnt9b*$^{fl/fl}$ (Carroll et al., 2005), *Klf4*$^{fl/fl}$ (Katz et al., 2002), *ROSA*^{EYFP} (Madisen et al., 2010) and *Dermo1*^{Cre} (Sosic et al., 2003) animals have been previously described. For all experiments littermates lacking Cre were used as controls and all animals were on a mixed background. Embryonic ages for each experiment are indicated in the figured legends, and embryo genders were unknown at the time of harvest. All animals were housed in a pathogen-free environment in an AAALAC-approved vivarium at the University of Pennsylvania, and experiments were performed in accordance with the guidelines of the Committee for Animal Research.

Zebrafish

Zebrafish lines used in this study were *Tg(klf2a*^{ig4}*)* (Steed et al., 2016), *vlad tepes*^{m651} (*gata1*) (Lyons et al., 2002), and *tnnt2a*^{tc300b} (Sehnert et al., 2002). All zebrafish experiments were approved by the Animal Experimentation Committee of the Institutional Review Board of the IGBMC.

Cell Culture

Pooled human microvascular endothelial cells HMVECs (Lonza) were grown in endothelial basal medium supplemented with EGM-2 MV SingleQuots (Lonza). HMVECs were infected overnight with LacZ (Penn Vector Core) KLF2 (Penn Vector Core) KLF4 (Vector Biolabs), or NFATC1 (Penn Vector Core) adenovirus at an MOI of 5. Forty-eight hours after infection, total RNA was isolated using TRIzol Reagent (Invitrogen). cDNA was generated from 1 μg total RNA using Superscript III Reverse Transcriptase (Invitrogen). qPCR was performed in Power SYBR Green PCR Master Mix (Applied Biosciences).

METHOD DETAILS

Histology and Immunohistochemistry

Mouse embryos were fixed in 4% paraformaldehyde(PFA) overnight at 4°C, dehydrated to 100% ethanol, and embedded in paraffin. Sections (7μm thick) were used for immunohistochemistry and haematoxylin and eosin staining. The following antibodies were used for immunostaining: goat anti-GFP (1:250, AbCam), rat anti-BrdU (1:100, AbCam), mouse anti-MF-20 (1:20, HybridomaBank), rabbit anti-RFP (1:250, Rockland), anti-KLF4 (1:100, R&D), rat anti-PECAM (1:50; HistoBioTec DIA-310), mouse anti-fibronectin (1:100, Santa Cruz) and mouse anti-NFATC1 (1:50, BDPharminagen). Images were taken on a Nikon Eclipse 80i fluorescent microscope (Nikon).

In Situ Hybridization

Probes for mouse *Wnt9b in situ* hybridization were generated by PCR amplification of kidney cDNA using previously designed primers (Alfieri et al., 2010). *In situ* hybridization was done as previously reported (Lee et al., 2006). For zebrafish whole mount *in situ* hybridization studies the pUC57 containing full length *wnt9b* cDNA (NM_001137660) (NovoPro) was used to subclone the *wnt9b* cDNA into pGEMt-easy vector using the following primers: forward 5'-TATTGCCCTCTGCATCCTTC-3' and reverse

5'-TGACATTCAACGTGACAGCA-3'. After digestion by NcoI, anti-sense DIG probe synthesis was done using Sp6 polymerase. *In situ* hybridizations were performed as previously described (Thisse and Thisse, 2008). In brief, embryos were placed in 24 well plate baskets containing 100% methanol then rehydrated to PBST. Permeabilization was achieved using proteinase K (10 μg/mL diluted in PBST) at room temperature for 30 min, followed by post-fixation in 4% PFA for 20 min. Embryos were then washed in PBST and then incubated with pre-warmed hybridization mix (50% Formamide, 5% SSC, 50 μg/ml Heparin, 500 μg/ml tRNA, 0.1% Tween-20, 0.92% 1M citric acid pH6 in water) for a minimum of 3 hours at 70°C. The hybridization mix was then replaced by 200 μL of hybridization mix supplemented with 2 μl of *wnt9b* probe and incubated overnight at 70°C. Embryos were washed by successive washes of 10 min each in MH buffer (50% formamide, 25% 20X SSC, 0.5% Tween-20, 0.92 % Citric acid 1M pH6 in water) 75% (vol/vol), 50% (vol/vol), 25% (vol/vol) MH buffer in 2X SSC, 100 % 2X SSC and 0.2X SSC for 30 min at 70°C. Then samples were washed in 75% (vol/vol), 50% (vol/vol), 25% (vol/vol) 0.2X SSC in PBST and finally in 100% PBST every 10 min at room temperature. Embryos were incubated in 20% blocking solution (Roche) in PBST for 3h at room temperature and then incubated overnight at 4°C in anti-DIG (alkaline phosphatase antibody, 1:10000, Roche) in 20% blocking solution with gentle rocking. The next day, embryos were washed in PBST at room temperature and placed in revelation solution (10% Tris-HCl 1M pH9.5, 5% $MgCl_2$ 1M, 2% NaCl 5M, 0.5% Tween-20 in water). Revelation was done at room temperature in BM-purple (Sigma). Embryos were washed in PBST several times and fixed in 4% PFA for storage. For RNAscope analysis, 48 and 56hpf wildtype zebrafish embryos were fixed in 4% PFA overnight at 4°C. The fixed embryos were dehydrated to 100% ethanol, embedded in paraffin and cut into 6 μm thick sections. Sections were stained using the RNAscope Fluorescent Multiplex kit (Advanced Cell Diagnostics).

In Vivo BrdU Incorporation Assay

Pregnant mice were injected intraperitoneally with 10 μg/g BrdU (Sigma) for 1 hour prior to embryo harvest. Paraffin sections were immunostained with anti-BrdU (1:100; AbCam) antibodies and nuclei visualized with DAPI. Quantitation of BrdU was performed by dividing the number of BrdU+ cells within a 7 μm AV valve section by the total number of DAPI positive cells in the same section. BrdU percentages were averaged from multiple AV valve sections per animal.

Cushion Quantitation

To examine KLF2-GFP intensity across the valve, GFP stained sections were converted to 8-bit and a line was drawn along the endocardium across the distance of the valve. Using ImageJ (NIH), image intensity across this line was then analyzed by generating a plot profile. To quantify intensity values, valves were divided into three sections, the area of the valve where the endocardium makes contact with the neighboring leaflet, and the two areas distal to this region. Gray values per pixel were generated from plot profiles of several AV sections per animal and were averaged from several analyzed sections. Quantitation of AV valve volume was performed by measuring the AV valve area of several HE sections and multiplying the sum of these areas by the tissue depth as determined by tissue section thickness. Quantitation of mesenchymal condensation was performed by counting the number of DAPI+ cells within a defined distance from the endocardium and dividing this by the cushion area included in this distance. Several AV valve sections were analyzed per animal and averaged.

Fetal Echocardiography

Pregnant mice were lightly anesthetized with 1-2% isoflurane and the uterus was exposed. *In utero* echocardiography was performed using a high-resolution micro-ultrasound system (VisualSonic Vevo 2100) with a 40 MHz mechanical transducer (MS550D). During scanning, maternal body temperature and heart rate were maintained within normal limits.

Optical Projection Tomography

E12.5 embryonic hearts were dissected and fixed overnight in 4% paraformaldehyde. Hearts were then embedded in 1% low-melt agarose, dehydrated in methanol, and then cleared in 1:2 (v/v) benzyl alcohol and benzyl benzoate as previously described (Sharpe et al., 2002). Organs were then scanned using the Bioptonics OPT Scanner (3001M) and color overlay of 2D images was done using Photoshop CS5.1.

Expression Studies

Total RNA was extracted from E12.5 AV cushions using the RNeasy Micro Kit (Qiagen). RNA quantity and quality were assayed with an Agilent 2100 Bioanalyzer (Agilent Technologies, Santa Clara, CA). Libraries were prepared using the TruSeq Stranded Total RNA Library Prep Kit with TruSeq RNA preparation kits with Ribo-Zero ribosomal RNA reduction chemistry (Illumina, San Diego, CA). 100bp single-read sequencing was performed on an Illumina HiSeq2500 sequencer in high output mode. Casava1.8.2 software was used for base calling (Illumina). GO analysis was performed by entering in the list of significantly changed genes into the gene ontology consortium (Release 20160715 (Ashburner et al., 2000; Gene Ontology Consortium, 2015)).

Casava1.8.2 software was used for base calling (Illumina). Low quality reads were filtered out as a first step. Next, ribosomal and repeat sequences were filtered out by alignment to a set of repeat sequences using the bowtie aligner (bowtie version 0.12.7), allowing 3 mismatches. Remaining reads were aligned to the mouse reference genome (NCBI build 37, mm9) and to the set of known transcripts included in RefSeq, UCSC known genes, and ENSEMBL transcripts, using RNA-Seq unified mapper (RUM) alignment software (University of Pennsylvania School of Medicine, Philadelphia, PA). RUM-computed transcript-, exon-, and intron-level quantitations of only uniquely aligning reads were used for further analysis.

To analyze global gene expression profiles, the number of uniquely aligning read counts to mRNA transcripts in RefSeq were extracted from the RUM output and processed for differential expression analysis. Pair-wise comparisons were carried out using a custom script implementing the EdgeR software (Walter and Eliza Hall Institute of Medical Research, Parkville, Australia). The *p*-values from EdgeR were corrected for multiple testing using the Benjamini & Hochberg mode of the R function p.adjust. Data was summarized for individual genes by selecting a ''representative transcript'' with the highest read counts for each gene. Intensity heatmap was generated using heatmap.2 function of R package gplots. Quantile normalized log2 expression values of genes were scaled on the mean log2 expression across samples and visualized on a color scale.

For validation of gene expression, total RNA was collected from whole E12.5 embryonic hearts. cDNA was synthesized from 150 ng total RNA using the Superscript III Reverse Transcriptase (Invitrogen). Real-time PCR was performed with Power SYBR Green PCR Master Mix (Applied Biosciences).

QUANTIFICATION AND STATISTICAL ANALYSIS

3-7 biological replicates were used for all experiments. All data were analyzed with GraphPad Prism (version 7) and represented as mean ± SEM. p values were calculated using an unpaired 2-tailed Student's t-test, or chi-square analysis as indicated in the figure legends. A p value less than 0.05 was considered statistically significant and is denoted as follows: *<0.05, **<0.01, ***<0.001 and ****<0.0001.

DATA AND SOFTWARE AVAILABILITY

The RNA-seq data set has been deposited in the NCBI GEO under accession number GEO: GSE80964.